nature cell biology

A mechanically active heterotypic E-cadherin/N-cadherin adhesion enables fibroblasts to drive cancer cell invasion

Anna Labernadie[1], Takuya Kato[2], Agustí Brugués[1], Xavier Serra-Picamal[1,3], Stefanie Derzsi[2], Esther Arwert[2], Anne Weston[2], Victor González-Tarragó[1], Alberto Elosegui-Artola[1], Lorenzo Albertazzi[1], Jordi Alcaraz[3], Pere Roca-Cusachs[1,3], Erik Sahai[2,6] and Xavier Trepat[1,3,4,5,6]

Cancer-associated fibroblasts (CAFs) promote tumour invasion and metastasis. We show that CAFs exert a physical force on cancer cells that enables their collective invasion. Force transmission is mediated by a heterophilic adhesion involving N-cadherin at the CAF membrane and E-cadherin at the cancer cell membrane. This adhesion is mechanically active; when subjected to force it triggers β-catenin recruitment and adhesion reinforcement dependent on α-catenin/vinculin interaction. Impairment of E-cadherin/N-cadherin adhesion abrogates the ability of CAFs to guide collective cell migration and blocks cancer cell invasion. N-cadherin also mediates repolarization of the CAFs away from the cancer cells. In parallel, nectins and afadin are recruited to the cancer cell/CAF interface and CAF repolarization is afadin dependent. Heterotypic junctions between CAFs and cancer cells are observed in patient-derived material. Together, our findings show that a mechanically active heterophilic adhesion between CAFs and cancer cells enables cooperative tumour invasion.

Carcinomas often retain epithelial features such as cell–cell junctions and a limited ability to degrade the extracellular matrix (ECM)[1,2]. These features should limit their invasion; however, carcinoma cells can metastasize without requiring an epithelial-to-mesenchymal transition[2–4]. One solution to this paradox is that epithelial cancer cells exploit non-malignant stromal cell types to develop cooperative invasion strategies[5,6]. Cancer-associated fibroblasts (CAFs) are ideal stromal partners to enable collective cancer cell invasion[5,7,8]. CAFs can remodel the ECM to create tracks for cancer cells to migrate[5,9], but the mechanisms by which cancer cells enter CAF-generated tracks and migrate along them are unclear. One possibility is that cancer cells simply follow the paths of least mechanical resistance. CAFs and cancer cells might also use communication strategies to invade cooperatively. One of these communication strategies could be the secretion of soluble growth factors and chemokines so as to generate chemotactic gradients to direct cell migration[10–14]. Contact-mediated signalling via Eph/ephrin or nectin/afadin complexes may also play a role in cancer cell–CAF communication[15,16]. Yet another possibility is that CAFs and cancer cells guide each other through mechanical interactions. Mechanical coupling of epithelial cells via E-cadherin and catenin complexes linked to the actin cytoskeleton is well established[17–21]. However, cadherin contacts between different cell types in pathological contexts have not been deeply studied, and almost nothing is known about mechanical coupling between CAFs and epithelial cancer cells.

Here we show that CAFs drive the collective invasion of cancer cells through an intercellular physical force. Unexpectedly, this physical force is transmitted through a heterophilic adherens junction involving E-cadherin on the cancer cell membrane and N-cadherin on the CAF membrane. Heterotypic adhesion between both cell types mediates not only force transmission and mechanotransduction but also CAF polarization.

RESULTS

CAFs lead cancer cell invasion in 3D and 2D migration assays

Spheroids containing cancer cells (A431) and CAFs, both derived from human vulval squamous cell carcinoma (SCC), were embedded in a mixture of collagen and Matrigel (Fig. 1a–c). Over 60 h cells invaded the surrounding 3D ECM forming strands in which the leading cell was generally one CAF followed by several A431 cells (Fig. 1a–c

[1]Institute for Bioengineering of Catalonia, Barcelona 08028, Spain. [2]The Francis Crick Institute, 1 Midland Road, London NW1 1AT, UK. [3]Unitat de Biofísica i Bioenginyeria, Facultat de Medicina, Universitat de Barcelona, Barcelona 08036, Spain. [4]Institució Catalana de Recerca i Estudis Avançats (ICREA), Barcelona 08010, Spain. [5]Centro de Investigación Biomédica en Red en Bioingeniería, Biomateriales y Nanomedicina, Barcelona 08028, Spain. [6]Correspondence should be addressed to E.S. or X.T. (e-mail: erik.sahai@crick.ac.uk or xtrepat@ibecbarcelona.eu)

Received 17 November 2016; accepted 18 January 2017; published online 20 February 2017; DOI: 10.1038/ncb3478

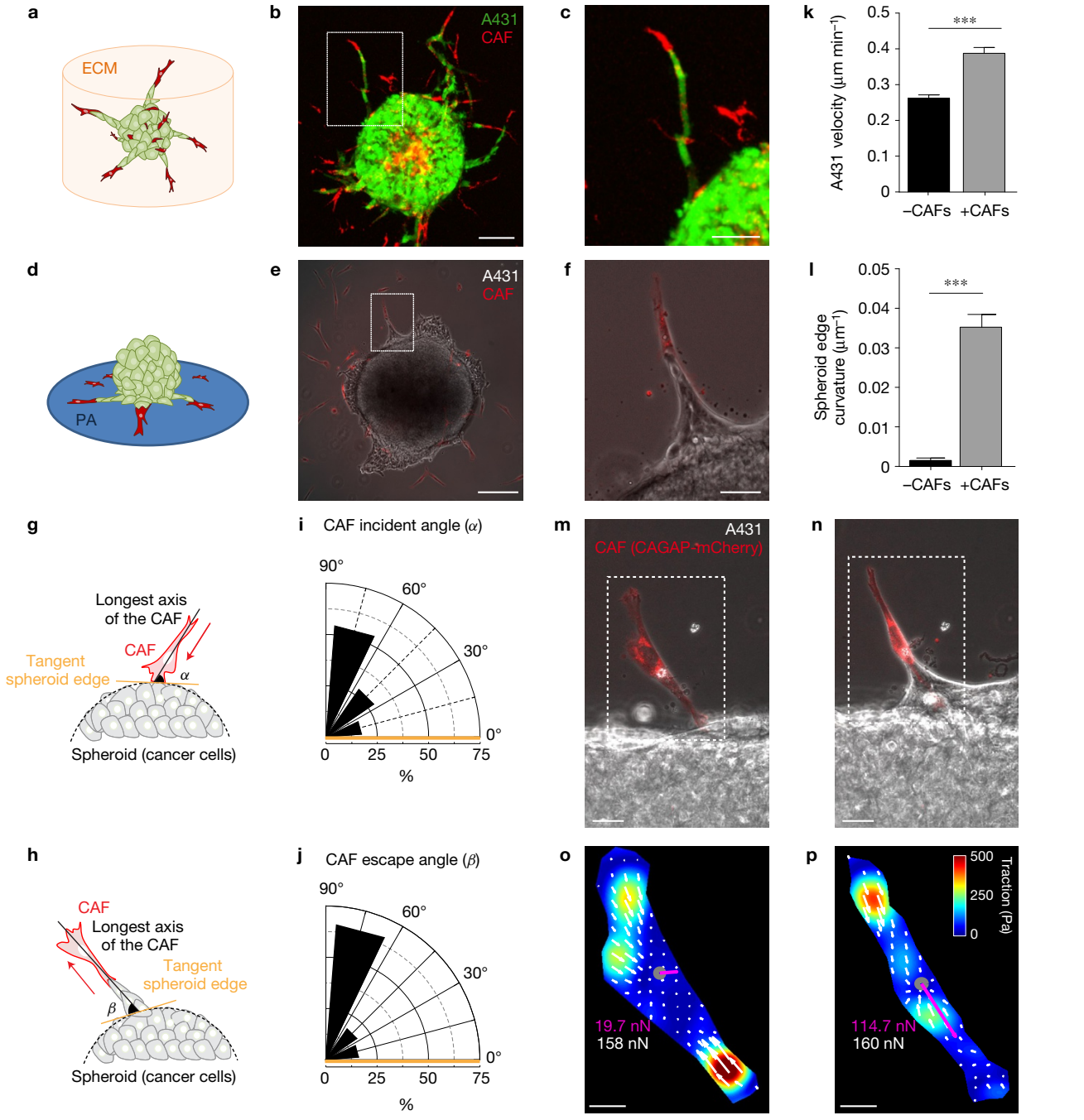

Figure 1 CAFs exert pulling forces on cancer cells. (**a**) Illustration of the 3D invasion assay (CAF, red; A431, green). (**b**) Confocal image of a spheroid (1:1 mixture of CAFs and A431 cells) after 60 h of invasion. CAFs (red) led collective strands of A431 cells (green). The image is representative of 6 samples. Scale bar, 100 μm. (**c**) Magnified view of the strand highlighted in **b**. Scale bar, 20 μm. (**d**) Illustration of the 2D migration assay. PA, polyacrylamide gel. (**e**) A spheroid of A431 cells (unlabelled) 10 h after CAF seeding (red). The image is representative of >10 samples. Scale bar, 100 μm. (**f**) Magnified view of the strand highlighted in **e**. Scale bar, 20 μm. (**g**) The incident angle (α) is defined as the angle between the longest axis of the CAF (black line) and the tangent to the spheroid edge (yellow line) at the first time of contact. By symmetry, α is taken in the range 0°–90°. (**h**) The escape angle (β) is defined as the angle between the longest axis of the CAF (black line) and the tangent to the spheroid after contact (yellow line). (**i**) Distribution of the incident angle α ($n=46$ CAFs from 3 independent experiments). (**j**) Distribution of the escape angle β ($n=47$ CAFs from 3 independent experiments). (**k**) Cancer cell velocity at the spheroid edge in the presence/absence of contact with CAFs. (**l**) Spheroid edge curvature in regions where CAFs contacted the spheroid (+CAF) and in regions of the same spheroid in which CAFs were absent (−CAF). In **k** and **l**, $n=177$ image fields without CAFs (−CAFs) and $n=40$ image fields with CAFs (+CAFs) from 5 independent experiments. (**m**,**n**) Merged image of a CAF (red) before (**m**) and 235 min after (**n**) contact with the spheroid edge (unlabelled). Scale bars, 10 μm. (**o**,**p**) Traction force maps of the CAFs in **m** and **n**, respectively. The purple vector indicates the magnitude and direction of the force transmitted at the interface between the CAF and the following A431 cell. The total traction force generated by the CAF is indicated in white and the force transmitted to the cancer cells is indicated in purple. Images and maps in **m**,**o** and **n**,**p** are representative of 12 and 13 samples, respectively. In **o**, the transmitted force falls within background noise levels (15.3 ± 9.4 nN, mean ± s.d.). Scale bars, 10 μm. Error bars represent s.e.m. $^{***}P<0.0001$, Mann–Whitney test.

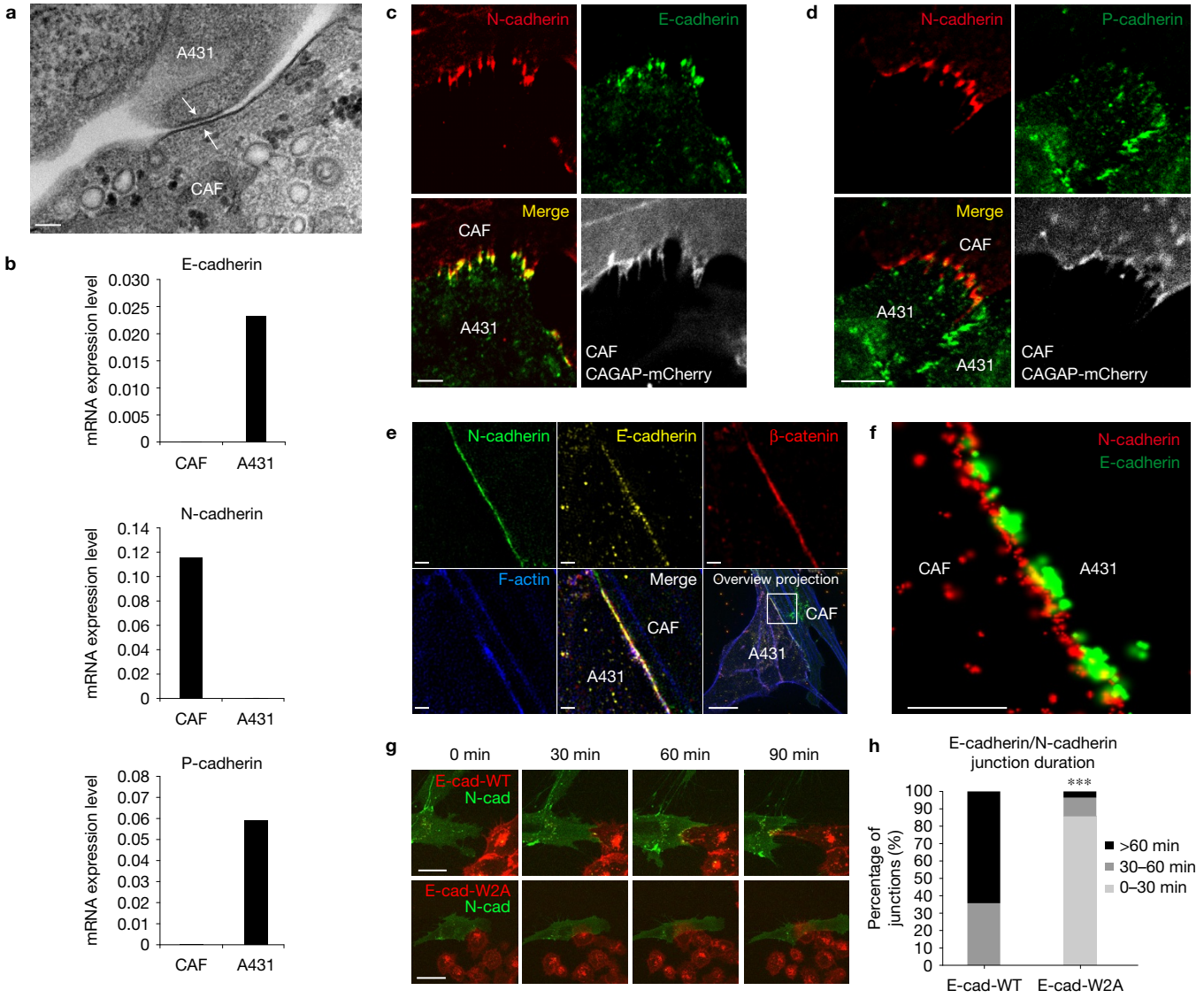

Figure 2 CAFs and A431 cells form heterophilic E-cadherin/N-cadherin junctions. (**a**) Transmission electron micrograph of contact (white arrows) between a CAF and a A431 cell. The image is representative of 20 contacts from 3 independent experiments. Scale bar, 100 nm. (**b**) mRNA expression levels of E-, N- and P-cadherin in CAFs and A431 cells measured using QRT–PCR. The bars show the average of technical triplicates. (**c**) Confocal immunofluorescence images of N-cadherin (red), E-cadherin (green) and CAGAP-mCherry (constitutively expressed by CAFs as a marker) in a co-culture of CAFs and A431 cells. The images are representative of >4 samples. Scale bar, 5 μm. (**d**) Confocal immunofluorescence images of N-cadherin, P-cadherin and CAGAP-mCherry (CAFs) in a co-culture of CAFs and A431 cells. The images are representative of >4 samples. Scale bar, 5 μm. (**e**) Structured illumination microscopy immunofluorescence images of N-cadherin (green), E-cadherin (yellow), β-catenin (red) and F-actin (blue) at a contact between a CAF and an A431 cell. The images are representative of 15 samples. Scale bars, 1 μm for zoomed areas, 10 μm for merged overview projection. (**f**) STORM image of N-cadherin/E-cadherin localization at the contact between a CAF and an A431 cell. The image is representative of 3 samples. Scale bar, 500 nm. (**g**) Time-lapse images of a CAF expressing N-cadherin-GFP contacting A431 cells expressing E-cadherin-WT (red) (upper panels) or A431 cells expressing E-cadherin-W2A mutant (red) (lower panels); scale bars, 20 μm. (**h**) Stacked histogram of the lifetime of the E-cadherin/N-cadherin junction (based on the E-cadherin and N-cadherin fluorescent signals) at the contact between CAFs and A431 cells, for CAFs mixed with A431-E-cad-WT cells (rescue control, $n = 14$ contacts from 3 independent experiments) and A431-E-cad-W2A mutant cells ($n = 28$ contacts from 3 independent experiments). Data are pooled in three categories of contact lifetime, from 0 to 30 min, from 30 to 60 min, and longer than 60 min duration. $^{***}P = 0.0007$, Chi-squared test.

and Supplementary Video 1)[5]. To study whether confinement by the ECM is required for the leader/follower organization of CAF/A431 invasion we designed a two-dimensional (2D) assay in which cells could migrate in the absence of the geometric constraints imposed by the ECM (Fig. 1d–f and Supplementary Videos 2 and 3). Spheroids containing only A431 cells were deposited on a soft polyacrylamide gels (Young's modulus, 6 kPa) and allowed to attach for ~12 h. We then added CAFs and let them attach randomly on the substrate. Within a few hours, a fraction of the CAFs contacted the spheroid (Supplementary Video 2). Following contact, CAFs inverted their front/rear polarity and migrated away from the spheroid followed by A431 cells (Fig. 1e,f and Supplementary Videos 2 and 3). To

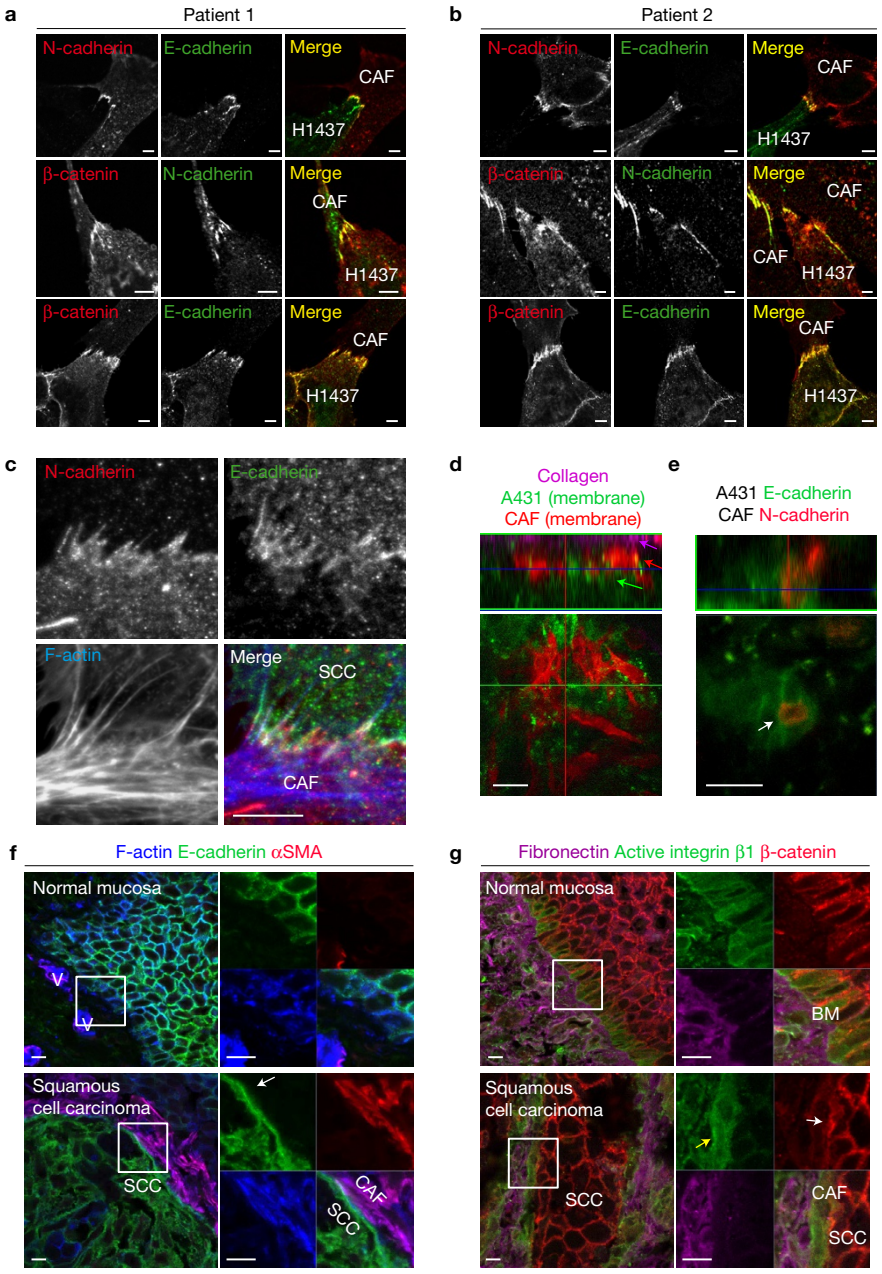

Figure 3 Evidence of E-cadherin/N-cadherin junctions in lung adenocarcinoma and vulval squamous cell carcinoma. (**a**,**b**) Co-cultures of CAFs from two patients with lung adenocarcinoma and H1437 cells show E-cadherin/N-cadherin junctions and β-catenin co-localization. The images are representative of 2 samples for each panel. Scale bars, 5 μm (see Supplementary Fig. 5 for a third patient). (**c**) Immunostaining of the contact between cancer cells and CAFs both isolated from one patient with vulval squamous cell carcinoma. The images are representative of 2 patient samples. Scale bar, 5 μm. (**d**) Panels show intravital imaging *xz* and *xy* sections of a tumour growing in the mouse ear: A431 (green), CAF (red), and collagen second harmonic (magenta); arrows highlight the different tumour components. The images are representative of 2 samples. Scale bar, 20 μm. (**e**) Panels show intravital imaging *xz* and *xy* sections of a tumour growing in the mouse ear: A431-E-cad-Ruby (shown in green) and vulval CAF-N-cad-GFP (shown in red). The white arrow highlights heterotypic contact. The images are representative of 3 samples. Scale bar, 20 μm. (**f**) Images show staining of F-actin (blue), E-cadherin (green) and αSMA (red) in normal human oral mucosa and oral squamous cell carcinoma. The white arrow highlights heterotypic contact between a CAF and a cancer cell; V, vessel. The images are representative of 5 samples. Scale bars, 10 μm. (**g**) Staining of fibronectin (magenta), active integrin β1 (green) and β-catenin (red) in normal human oral mucosa and oral squamous cell carcinoma. The white arrow highlights heterotypic contact between a CAF and a cancer cell; the yellow arrow highlights integrin/ECM contact by CAF; BM, basement membrane. The images are representative of 5 samples. Scale bars, 10 μm.

characterize CAF repolarization we took advantage of their elongated shape, and we defined the incident angle (α) as the angle between the CAF orientation and the tangent to the spheroid immediately before contact (Fig. 1g). Conversely, we defined the escape angle (β) as the angle between the CAF orientation and the tangent to the spheroid after contact (Fig. 1h). CAFs approached the spheroids following a

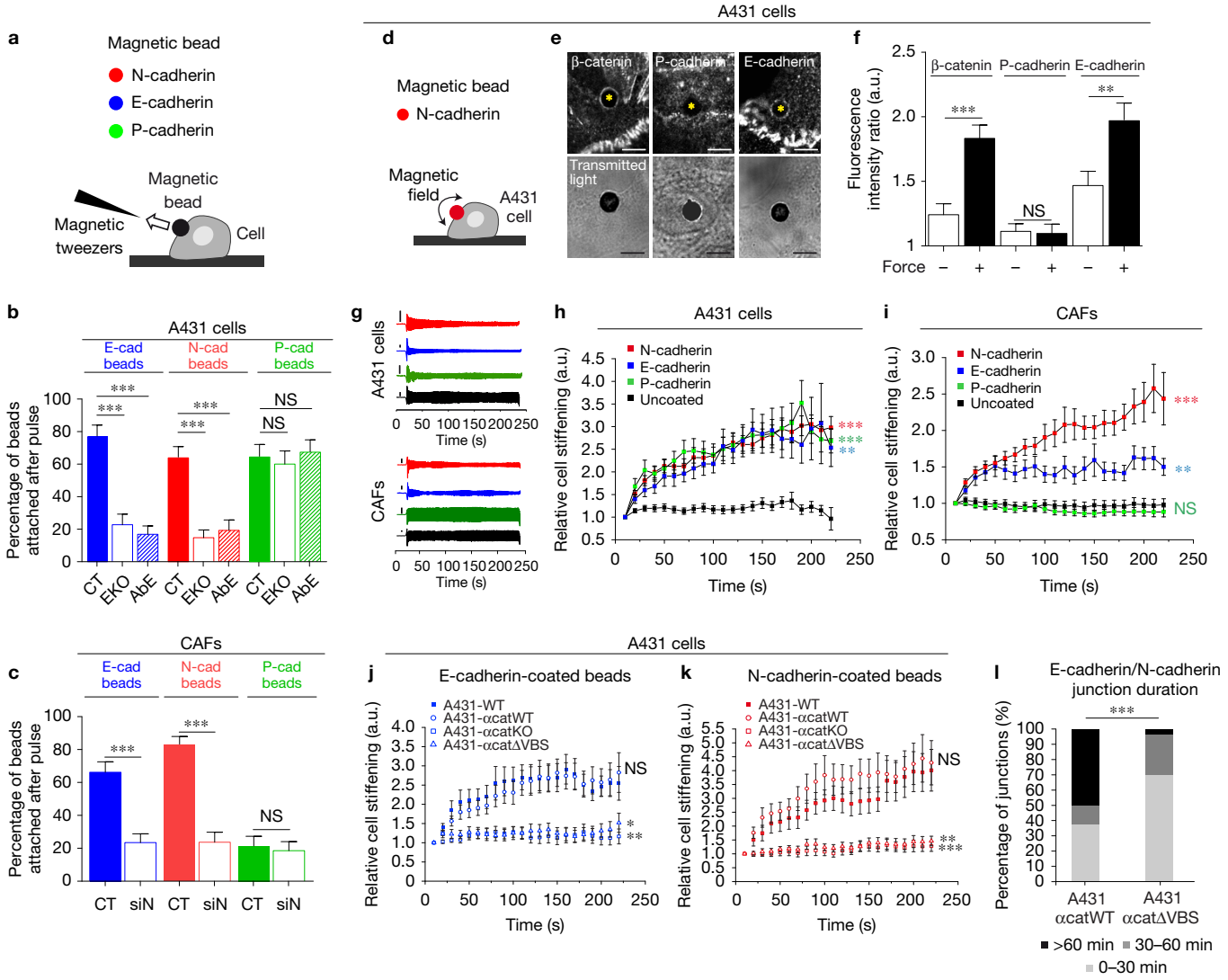

Figure 4 Heterophilic E-cadherin/N-cadherin junctions withstand forces and trigger mechanotransduction. (**a**) Illustration of the magnetic tweezers experimental set-up. (**b**) Bead detachment data in A431 cells (CT), A431-EcadKO cells (EKO) and A431 cells pre-treated with E-cadherin-blocking antibody (AbE). Percentage of beads coated with N-, E- and P-cadherin that remained attached to A431 cells after application of a force pulse. (**c**) Bead detachment data in CAFs transfected with siRNA control (CT) and CAF-siNcad (siN). Percentage of beads coated with N-, E- and P-cadherin that remained attached to CAFs after application of a force pulse. (**d**) Illustration of the magnetic twisting experimental set-up. (**e**) Representative fluorescence (top) and bright-field (bottom) images showing the recruitment of β-catenin, P-cadherin and E-cadherin in A431 cells subjected to magnetic stimulation using N-cadherin-coated magnetic beads. The yellow asterisks indicate the location of the beads. Scale bars, 5 μm. (**f**) Quantification of the recruitment of β-catenin, P-cadherin and E-cadherin mediated by N-cadherin-coated beads with/without (+/− force) mechanical stimulation. (**g**) Representative bead traces for A431 cells and CAFs in response to a series of force pulses applied to beads coated with N-cadherin (red), E-cadherin (blue), P-cadherin (green) or uncoated (black). Vertical bars, 200 nm. (**h**) Stiffening of the A431 cell–bead contact defined as the time evolution of the ratio between applied force and bead displacement relative to baseline (N-, E-, P-cadherin-coated beads, and uncoated beads). (**i**) Stiffening of the CAF–bead contact. (**j**) Stiffening of the cell/E-cadherin-coated bead contact for control A431 cells (A431-WT) and α-catenin mutants. (**k**) Stiffening of the cell/N-cadherin-coated bead contact for A431-WT cells and α-catenin mutants. (**l**) Stacked histogram of the lifetime of the E-cadherin/N-cadherin junction at the contact between CAFs and A431 cells, for CAFs mixed with A431-αcatWT cells and A431-αcatΔVBS cells. Data are pooled in three categories of contact lifetime, from 0 to 30 min, from 30 to 60 min, and above 60 min duration. See Supplementary Table 1 for sample numbers and statistical analysis. Error bars represent s.e.m.

trajectory that was generally perpendicular to the spheroid tangent (Fig. 1i). The escape trajectory was also perpendicular to the spheroid tangent, indicating an inversion of CAF polarity reminiscent of that observed during contact inhibition of locomotion (CIL)[15,22–26] (Fig. 1j and Supplementary Videos 2 and 3). Unlike cells undergoing CIL, and despite the absence of surrounding 3D ECM, CAFs remained in close contact with cancer cells in a leader/follower organization that lasted several hours. Both the velocity of A431 cells and the local curvature of the spheroid were highest in the regions where CAFs were leading the spreading of the spheroid (Fig. 1k,l). These results show that intercellular communication mechanisms independent of the 3D ECM must be invoked to explain guidance of cancer cells by CAFs.

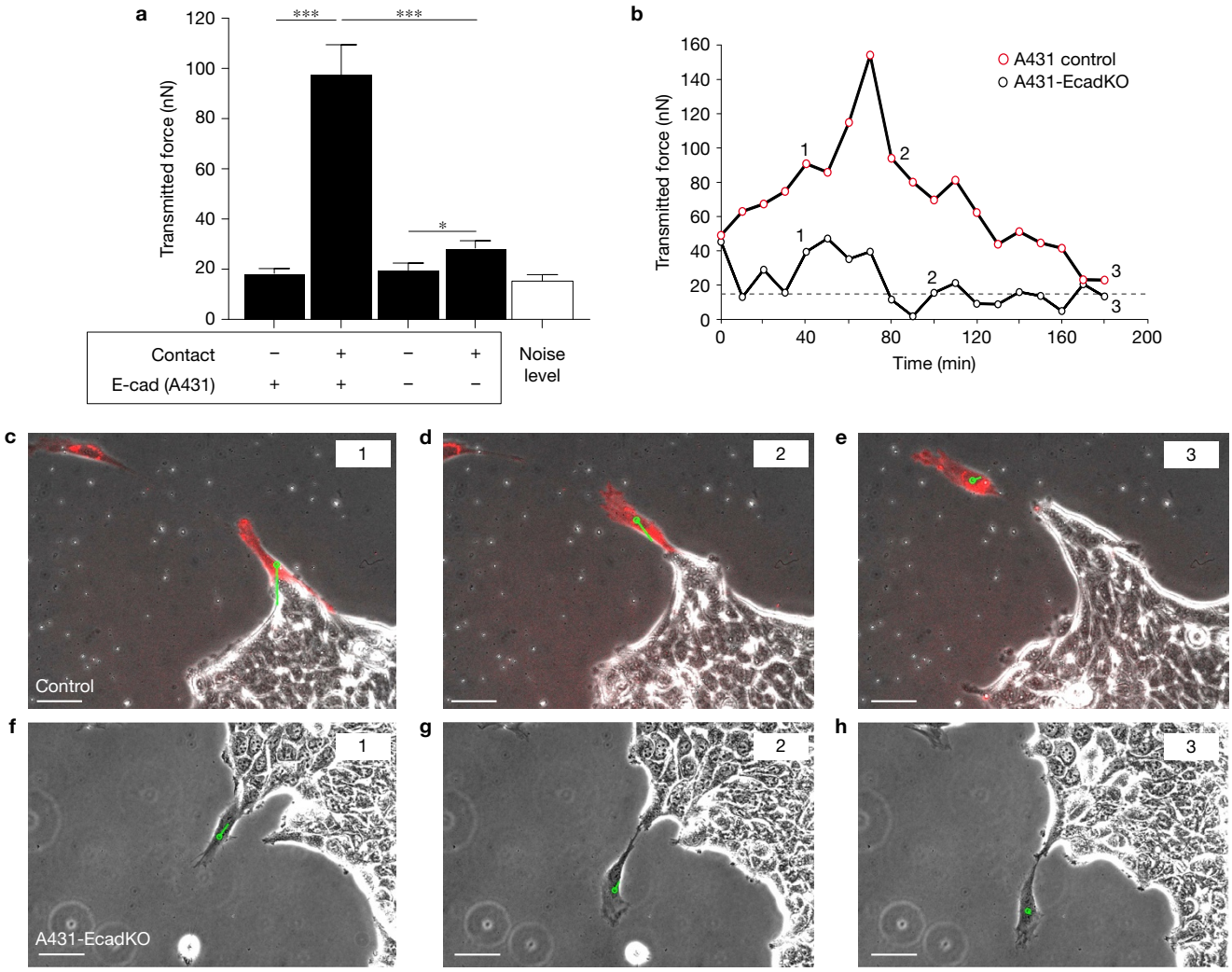

Figure 5 E-cadherin is required for force transmission between CAFs and A431 cells. (**a**) Net force transmitted between CAFs and A431 cells before the onset of contact and during contact. Experiments were performed under control conditions and after depletion of E-cadherin in the A431 cells using CRISPR/Cas9. The white bar indicates background noise level. '−/+' $n=12$ CAFs from 9 independent experiments, '+/+' $n=13$ CAFs from 9 independent experiments, '−/−' $n=13$ CAFs from 2 independent experiments, '+/−' $n=17$ CAFs from 2 independent experiments, $n=13$ image regions from 8 independent experiments (noise level). Error bars represent s.e.m. $^{***}P<0.0001$, $^{*}P=0.0409$, unpaired two-tailed t-test. (**b**) Time evolution of the transmitted force between a CAF and the follower cancer cell for control A431 (red open symbols) and A431-EcadKO (black open symbols). The dashed line indicates the noise floor. (**c**–**e**) Snapshots of the collective migration of control A431 cells led by one CAF (CAGAP-mCherry) corresponding to the three time points labelled in **b**. The green vector indicates the magnitude and direction of the net transmitted force. The data are representative of 5 time-lapse experiments. See Supplementary Video 10 for the full time lapse. (**f**–**h**) Snapshots of the collective migration of control A431-EcadKO cells led by one CAF corresponding to the three time points labelled in **b**. See Supplementary Video 11 for the full time lapse. The data are representative of 5 time-lapse experiments. Scale bars, 50 μm.

CAFs generate pulling forces on cancer cells

Guidance of cancer cell migration by CAFs could result from paracrine signalling, as in the case of tumour-associated macrophages[6], but also by direct physical dragging through a force exerted by CAFs on cancer cells. To test the latter possibility, we used traction force microscopy to monitor forces generated by the CAFs on their substrate before contacting the spheroid (Fig. 1m,o) and during CAF-led migration (Fig. 1n,p). Before contact, CAFs exhibited a traction pattern characteristic of mesenchymal cells in isolation; forces were restricted to both edges of the CAFs and, within the experimental noise, the vectorial sum of forces vanished, indicating force balance (Fig. 1o). In contrast, when CAFs were leading cancer cell migration, traction forces exerted by CAFs were locally unbalanced and tractions at the leading edge largely exceeded those at the trailing edge (Fig. 1p). As a direct consequence of Newton's laws[17,27–30] this result establishes that traction forces generated by CAFs at the leading edge are transmitted to cancer cells.

CAFs and A431 cells form heterophilic E-cadherin/N-cadherin junctions

To be able to transmit forces, CAFs and cancer cells must be mechanically connected. This was confirmed by the observation of multiple contact points in transmission electron microscopy and focused ion beam scanning electron microscopy (FIB-SEM) (Fig. 2a

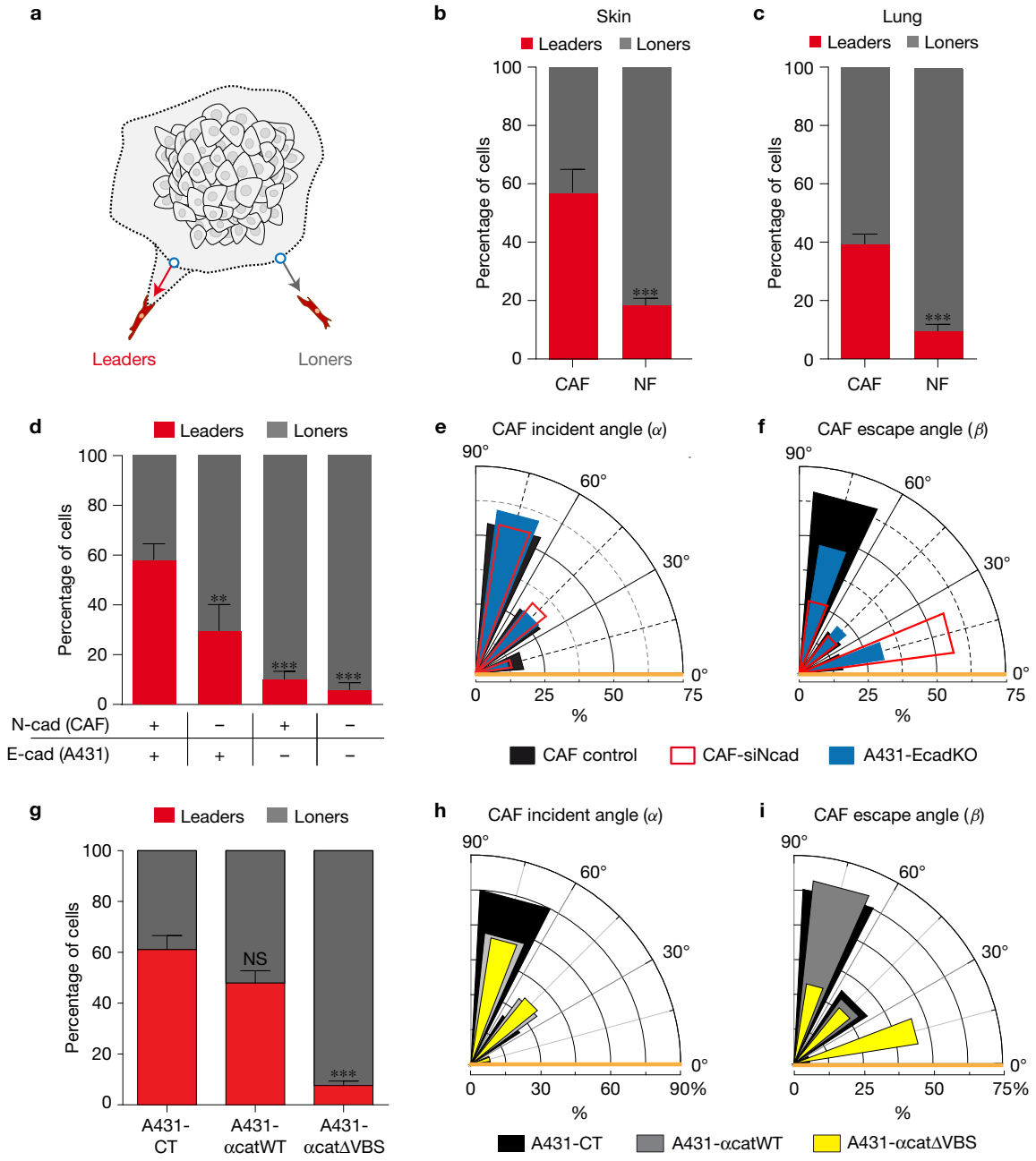

Figure 6 A mechanically active heterotypic adhesion regulates cell trajectories, leader/follower patterns, and CAF polarization. (**a**) Illustration of the two modes of 2D collective invasion. CAFs (red) were classified either as 'leaders' if their invasion was followed by a strand of A431 cells or as 'loners' if they migrated away from the spheroid (grey) as individual cells. (**b**) Fraction of 'leaders' versus 'loners' in dermal CAFs compared with normal dermal fibroblasts (NF, skin) paired with A431 cell spheroids. $n=57$ CAFs and 194 NFs from 3 experiments; $^{***}P<0.0001$. (**c**) Fraction of 'leaders' versus 'loners' in lung CAFs compared with normal lung fibroblasts paired with H1437 cell spheroids. $n=202$ CAFs and 192 NFs from 3 experiments; $^{***}P<0.0001$. (**d**) Fraction of 'leaders' versus 'loners' on depletion of the E-cadherin/N-cadherin junction ('+/+' $n=86$ CAFs from 4 experiments, '−/+' $n=30$ CAFs from 4 experiments ($P=0.006$), '+/−' $n=67$ CAFs from 3 independent experiments ($P<0.0001$), '−/−' $n=76$ CAFs from 3 experiments ($P=0.001$)). (**e**) Distribution of the incident angle α for control CAFs ($n=46$ CAFs), CAF-siNcad ($n=46$ CAFs) and A431-EcadKO ($n=42$ CAFs), all pooled from 3 experiments. Distributions were not significantly different from each other. (**f**) Distribution of the escape angle β for control CAFs ($n=44$ CAFs), CAF-siNcad ($n=53$ CAFs) and A431-EcadKO ($n=35$ CAFs), all pooled from 3 experiments. The escape angle distribution for CAF-siNcad and A431-EcadKO was significantly different from that of CAF control ($P<0.001$ for CAF-siNcad and $P<0.05$ for A431-EcadKO). (**g**) Fraction of 'leaders' versus 'loners' in CAFs paired with a A431-CT ($n=106$ CAFs), A431-αcatWT ($n=194$ CAFs, $P=0.098$) and A431-αcatΔVBS ($n=248$ CAFs, $P<0.0001$). The data are pooled from 3 experiments. (**h**) Distribution of the incident angle α for control CAFs paired with A431-CT ($n=36$ CAFs), A431-αcatWT ($n=60$ CAFs) and A431-αcatΔVBS ($n=62$ CAFs), all pooled from 3 experiments. Distributions were not significantly different from each other. (**i**) Distribution of the escape angle β for A431-CT ($n=36$ CAFs), A431-αcatWT ($n=60$ CAFs) and A431-αcatΔVBS ($n=62$ CAFs), all pooled from 3 experiments. The escape angle distribution for A431-αcatΔVBS was significantly different from that of A431-CT. All other distributions were not significantly different from each other. $^{***}P<0.001$, $^{**}P<0.01$; NS, not significantly different. **b**–**d**,**g**, Mann–Whitney test; **e**,**f**,**h**,**i**, Kolmogorov–Smirnov test. Error bars represent s.e.m.

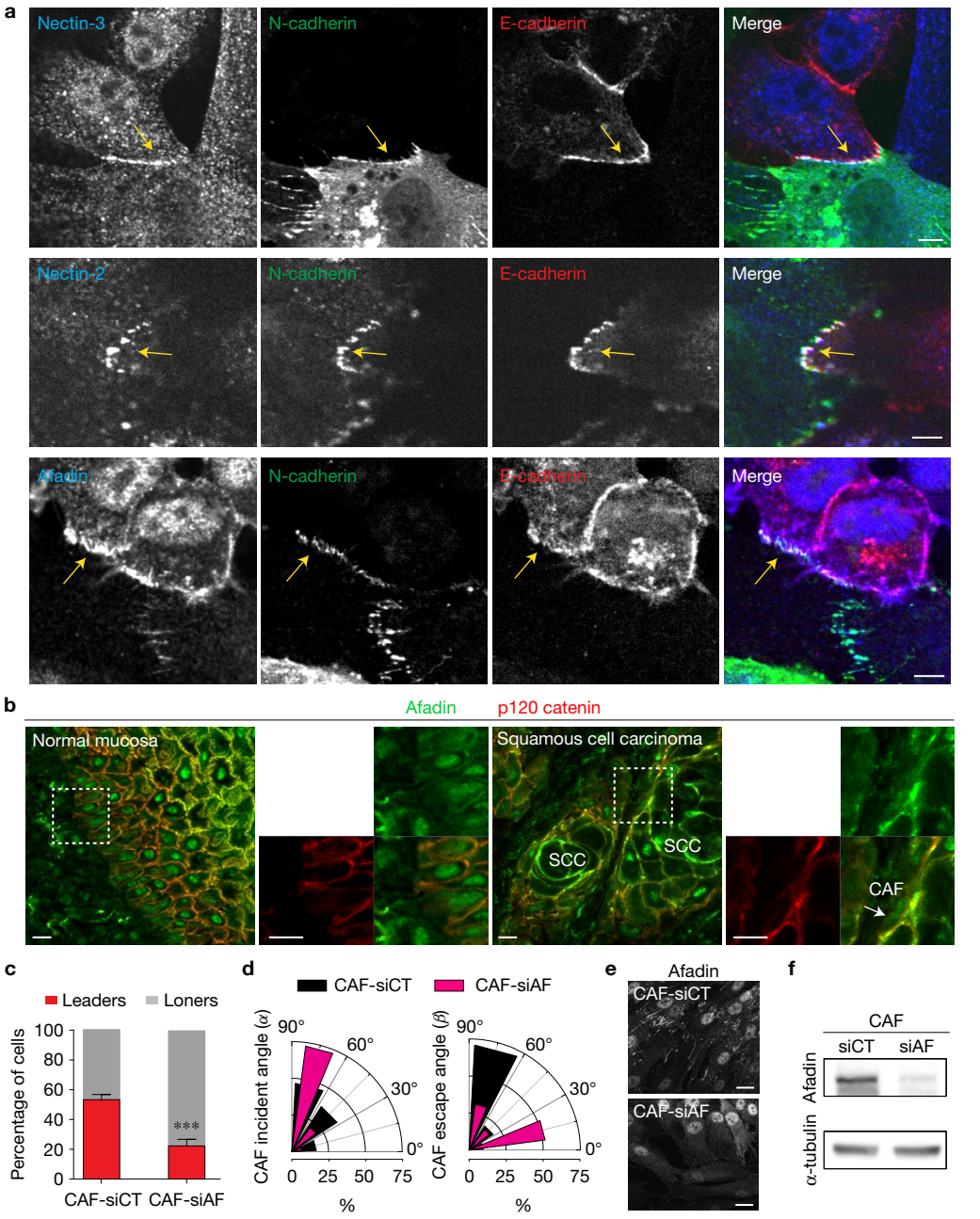

Figure 7 Afadin and nectins 2 and 3 are required for CAF-led migration of cancer cells and for CAF polarization. (**a**) Confocal images of nectin-3 (blue), N-cadherin (green) and E-cadherin (red) in a co-culture of CAFs and A431 cells (upper panels); nectin-2 (blue), N-cadherin (green) and E-cadherin (red) (middle panels); afadin (blue), N-cadherin (green) and E-cadherin (red) (lower panels). The yellow arrows show the localization of the CAF/A431 cell contact. The images are representative of 2 samples. Scale bars, 5 μm. (**b**) Staining of afadin (green) and p120catenin (red) in normal human oral mucosa and oral squamous cell carcinoma. The white arrow highlights heterotypic contact between a CAF and a cancer cell. The images are representative of 5 samples. Scale bars, 10 μm. (**c**) Fraction of 'leaders' versus 'loners' in CAF-siCT ($n=90$ CAFs) and CAF-siAF ($n=95$ CAFs). The data are pooled from 3 independent experiments. $^{***}P<0.001$, *t*-test. (**d**) Distribution of the incident angle α and escape angle β for CAF-siCT ($n=30$, 32 CAFs for α and β, respectively) and CAF-siAF ($n=29$ CAFs for α and β), all pooled from 3 independent experiments. Escape angle distribution of CAF-siAF was significantly different from that of CAF-siCT ($P=0.0001$ Kolmogorov–Smirnov test). All other distributions were not significantly different from each other. (**e**) Confocal fluorescence images of afadin staining in CAFs 3 days after siRNA transfection with siRNA control or siRNA targeting afadin. The images are representative of 3 samples. Scale bars, 20 μm. (**f**) Western blot of afadin and α-tubulin for CAF-siCT and CAF-siAF. Unprocessed original scans of blots are shown in Supplementary Fig. 9.

and Supplementary Video 4). To identify the proteins involved in these interactions, we first focused on classical cadherins (E-, N-, P-cadherin). Quantitative PCR with reverse transcription (QRT–PCR) analysis revealed that A431 cells expressed both E- and P-cadherin, consistent with previous results[31], and CAFs expressed N-cadherin (Fig. 2b). This excludes the possibility of homophilic interactions

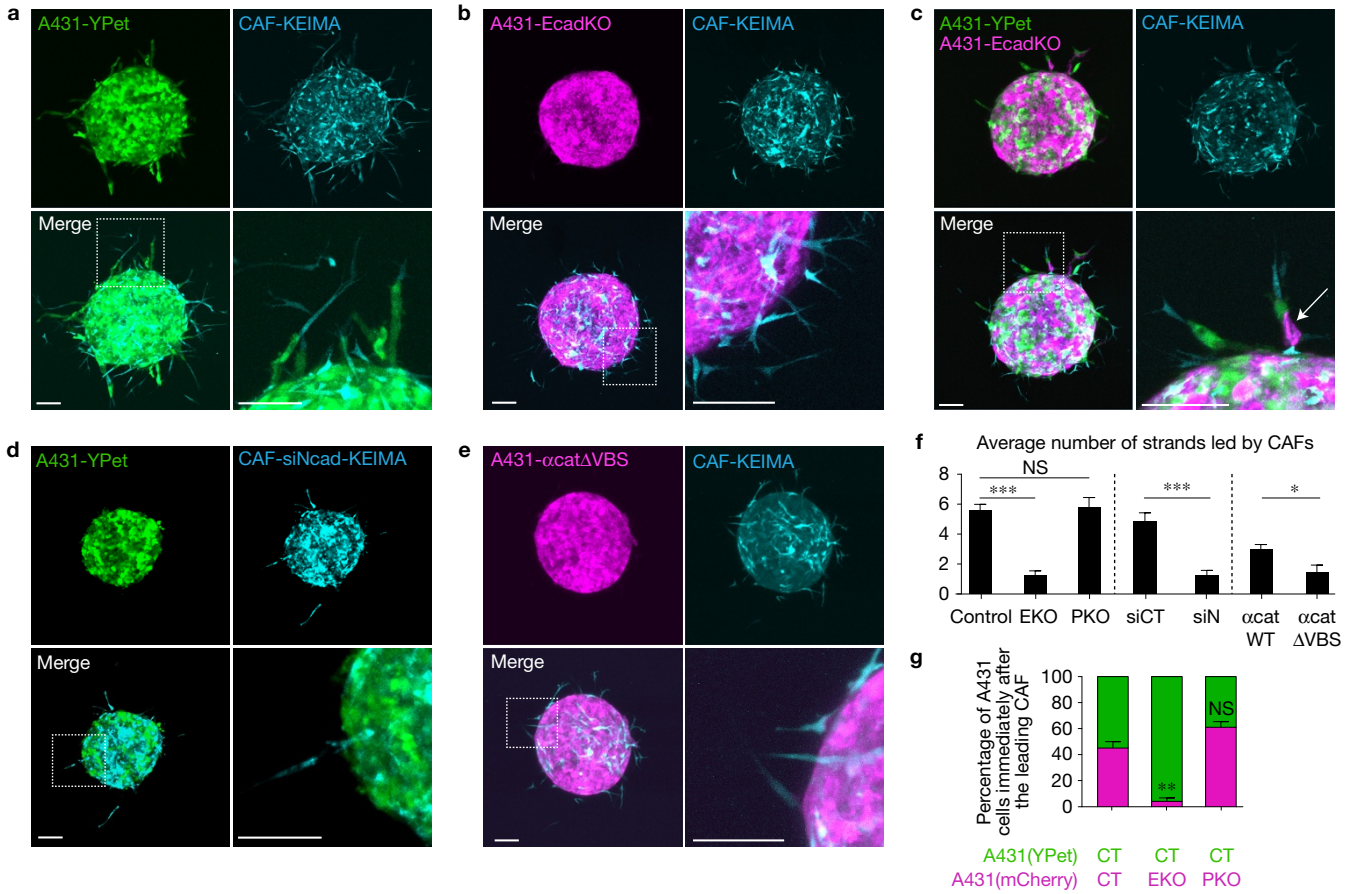

Figure 8 The E-cadherin/N-cadherin junction enables collective cancer cell invasion in 3D. (**a**–**e**) Fluorescence images of spheroids containing different mixtures of CAFs and A431 cells after 60 h of invasion in an organotypic ECM. (**a**) 1:1 mixture of control A431 (YPet) and control CAFs (KEIMA). (**b**) 1:1 mixture of A431-EcadKO (mCherry) and control CAFs (KEIMA). (**c**) 1:1:2 mixture of A431-control (YPet), A431-EcadKO (mCherry) and control CAFs (KEIMA). The arrow points to one A431-EcadKO cell in the invasive strand. (**d**) 1:1 mixture of A431-control (YPet) and CAF-siNcad (KEIMA). (**e**) 1:1 mixture of A431-αcatΔVBS cells (mCherry) and CAFs-siRNA (KEIMA). See Supplementary Fig. 7 for additional spheroid conditions. Scale bars, 100 μm. (**f**) Average number of strands per spheroid in the conditions shown in **a**–**e**, and CAF-siCT and A431-αcatWT. Number of spheroids measured: $n = 24$ (control), $n = 18$ (EKO, $^{***}P < 0.0001$), $n = 18$ (PKO, $P > 0.999$), $n = 19$ (siCT), $n = 19$ (siN, $P < 0.0001$), $n = 11$ (αcatWT), 6 (αcatΔVBS, $^{*}P = 0.016$), from 3 independent experiments. One-way ANOVA with Dunn's multiple comparison test. (**g**) Percentage of the A431 cells found immediately after the CAFs in spheroids containing a triple mixture of two distinct populations of A431 (YPet, mCherry) and one population of CAFs (KEIMA). The three combinations of A431 cells are: A431-control (Ypet)/A431-control (mCherry) ($n = 66$ strands measured), A431-control (YPet)/A431-EcadKO (mCherry) ($n = 41$ strands measured, $P = 0.0024$), and A431-control (YPet)/A431-PcadKO (mCherry) ($n = 56$ strands measured, $P = 0.826$), from 3 independent experiments. These results show that when A431-control cells and A431-EcadKO cells are mixed, the probability of finding an A431-EcadKO behind the leading CAF is negligible. Error bars are s.e.m; NS, not significantly different when compared to controls. One-way ANOVA with Dunn's multiple comparison test.

between CAFs and A431 cells involving classical cadherins. We therefore considered the possibility of heterophilic junctions between N-cadherin at the CAF membrane and E- or P-cadherin at the A431 membrane. Co-cultured CAFs and cancer cells showed co-localization of E-cadherin and N-cadherin at contacts between the two cell types (Fig. 2c and Supplementary Fig. 1a–e). Further, α-catenin, β-catenin and vinculin were observed at the interface between A431 cells and CAFs (Supplementary Figs 2 and 3). Higher-resolution structured illumination microscopy and stochastic optical reconstruction microscopy (STORM) confirmed the co-localization of E-cadherin, N-cadherin, β-catenin and F-actin (Fig. 2e,f and Supplementary Fig. 1f). P-cadherin localized at the junctions between A431 cells, but not between CAFs and A431 cells (Fig. 2d and Supplementary Fig. 1g).

To study junctional kinematics we stably expressed N-cadherin-EGFP in CAFs and E-cadherin-Ruby in A431 cells deleted for endogenous E-cadherin using CRISPR/Cas9 (details in Supplementary Fig. 4a–g,q). E-cadherin and N-cadherin co-localized within 30 min of contact between cells, and this co-localization persisted for >60 min (Fig. 2g,h). In contrast, expression of E-cadherin with a W2A mutation in the extracellular domain (A431-EcadW2A) drastically diminished co-localization with N-cadherin, and the few contacts that formed were short-lived (Fig. 2g,h and Supplementary Video 5). This suggests that E-cadherin and N-cadherin form strand-swap dimers between their cadherin EC1 domains[32,33]. Calcium chelation and re-addition experiments confirmed the importance of Ca^{2+} for E-cadherin/N-cadherin co-localization (Supplementary Video 6). Further time-lapse imaging confirmed the localization

with β-catenin and vinculin at E-cadherin/N-cadherin junctions (Supplementary Videos 7–9).

E-cadherin/N-cadherin heterophilic junctions between CAFs and cancer cells are present in different types of carcinoma

We next investigated whether the E-cadherin/N-cadherin junction was present in other types of carcinoma (Fig. 3). We analysed co-cultures of primary human CAFs isolated from lung adenocarcinoma patients and human lung adenocarcinoma cancer cells (H1437). Similarly to A431 cells, H1437 are weakly invasive carcinoma cells that express E-cadherin, but not N-cadherin or P-cadherin[34]. In the three patients analysed, immunostainings revealed the extensive presence of E-cadherin/N-cadherin junctions and their systematic co-localization with β-catenin (Fig. 3a,b and Supplementary Fig. 5). We also co-cultured cancer cells and CAFs isolated from the same vulval squamous cell carcinoma patient. These experiments also showed co-localization of N-cadherin, E-cadherin and F-actin at the CAF–cancer cell contact (Fig. 3c).

To investigate heterotypic contacts between cancer cells and fibroblasts *in vivo* we performed intravital imaging and analysed patient samples. Figure 3d,e shows close contact of cancer cells and CAFs in tumours generated by the co-injection of A431 cells and CAFs. CAFs were typically located at the tumour margin between the cancer cells and the ECM (magenta in *xz* projection). Co-injection of E-cadherin-Ruby A431 cells and N-cadherin-GFP CAFs revealed co-location of both cadherins at the interface between cancer cells and CAFs (Fig. 3e). More significantly, staining of human squamous cell carcinoma revealed clear localization of E-cadherin at the interface between cancer cells and α-smooth muscle actin (αSMA)-positive CAFs (Fig. 3f). β-catenin was also localized at this interface (Fig. 3g); as expected, neither E-cadherin nor β-catenin localized to the basal surface of normal epidermis. In addition to analysing heterotypic cell contacts, we investigated cell–ECM contacts by staining for active integrin β1 and fibronectin. This revealed rather variable cell–ECM contacts in SCC cells. CAFs showed higher levels of integrin activation and fibronectin contact and, in some cases, CAFs were simultaneously making contact with the ECM and cancer cells (yellow and white arrows, respectively, in the right-hand panel of Fig. 3g). Thus, heterotypic E-cadherin/N-cadherin junctions are observed in many contexts in both lung and squamous cell carcinoma.

The E-cadherin/N-cadherin junction withstands similar forces to homophilic junctions

To address the mechanical properties of a heterotypic E-cadherin/N-cadherin contact, we employed a set of magnetocytometry approaches[19,35–37] to apply forces on beads attached to cells through diverse homophilic and heterophilic cadherin adhesions (Fig. 4). We coated magnetic beads with either recombinant E-, N- or P-cadherin–Fc fusion proteins and allowed them to attach to A431 cells (Fig. 4a). We quantified the number of beads attached to cells after applying a pulling force of 0.5 nN for 1 min (Fig. 4b). After the force pulse, ∼70% of the beads coated with either E-cadherin or P-cadherin remained attached to the cells, thus indicating a similar strength of homophilic E-cadherin and P-cadherin adhesions in A431 cells. Despite the fact that A431 cells do not express N-cadherin, ∼70% of the beads coated with N-cadherin also resisted the force pulse, indicating that the heterophilic N-cadherin junction with A431 cells was able to withstand similar forces as the homophilic E-cadherin/E-cadherin junctions.

We next repeated the protocol using A431-EcadKO cells. E-cadherin knockout did not lead to compensatory expression of N-cadherin, although P-cadherin levels increased modestly (Supplementary Fig. 4a). As expected, the binding of E-cadherin beads decreased very significantly, although some residual nonspecific interaction remained[37] (Fig. 4b). The number of P-cadherin beads that resisted the force pulse did not change in A431-EcadKO cells, thus highlighting the specificity of the assay. Importantly, knocking out E-cadherin resulted in a large drop in N-cadherin bead binding, which supports the existence of a heterophilic adhesion between N-cadherin and E-cadherin (Fig. 4b). To confirm the E-cadherin dependence of N-cadherin binding, we used an E-cadherin blocking antibody (Fig. 4b). These experiments paralleled those in A431-EcadKO cells, further supporting that adhesion of N-cadherin beads to A431 cells is mediated by heterophilic contact with E-cadherin.

We applied the same experimental approach to CAFs (Fig. 4c). The majority of N-cadherin beads (∼80%) remained attached after the magnetic pulse, whereas most P-cadherin beads were unable to resist the applied force. A large fraction (63%) of beads coated with E-cadherin remained attached to the CAF surface, consistent with a heterotypic E-cadherin/N-cadherin junction. To further investigate this interaction in CAFs, we used short interfering RNA (siRNA) to knockdown N-cadherin (CAF-siNcad, see Supplementary Fig. 4f,h-k,n,q) and repeated the pulse application. In these experiments, the number of E-cadherin and N-cadherin beads that remained attached decreased to residual levels. We conclude that both A431 cells and CAFs are able to form strong heterotypic adhesions through E-cadherin and N-cadherin.

The E-cadherin/N-cadherin junction is mechanosensitive

We next studied whether the junction is mechanosensitive. We first investigated whether adherens junction proteins are recruited to the membrane of A431 cells when exposed to a bead coated with N-cadherin (Fig. 4d–f). Immunostainings of the cell–bead contact revealed accumulation of β-catenin and E-cadherin but not P-cadherin, indicating that N-cadherin is sufficient to recruit E-cadherin and actin-binding partners (Fig. 4e,f). We then applied a pulsatile force to the cell–bead contact and observed a significant increase in the recruitment of β-catenin and E-cadherin but not of P-cadherin (Fig. 4f). These results establish that a heterophilic E-cadherin/N-cadherin junction triggers a specific mechanotransduction response.

To quantify the mechanical response of the E-cadherin/N-cadherin junction we used magnetic tweezers to apply high pulsatile forces to the adherent magnetic beads and recorded the resulting bead displacements[19,21,35] (Fig. 4g–i). In A431 cells, pulling on E- and P-cadherin beads resulted in a progressive decrease in bead displacements, showing that cells responded to the applied force by stiffening the adhesion (Fig. 4g,h). No stiffening was observed when pulling on uncoated beads, indicating that unspecific binding of the beads does not induce a mechanoresponse. Despite the fact that A431 cells do not express N-cadherin, force applied to N-cadherin beads also triggered reinforcement of the adhesion with similar magnitude and time evolution as those of homophilic

E- and P-cadherin adhesions. We followed the same approach to analyse mechanosensitivity of the E-cadherin/N-cadherin junction in CAFs (Fig. 4g,i). As expected, force applied to N-cadherin-coated beads triggered strong reinforcement of the CAF–bead contact. Force applied through E-cadherin beads also triggered mechanical reinforcement in CAFs, although to a lesser extent than N-cadherin beads. Force applied through P-cadherin beads or uncoated beads unspecifically bound to the CAFs did not affect dynamics of the cell–bead contact. Taken together, our results establish that, unlike previously thought[35], a heterophilic E-cadherin/N-cadherin adhesion is able to sense and actively respond to physical forces.

Mechanotransduction at adherens junctions has been attributed to forced unfolding of a cryptic binding site in α-catenin that enables vinculin binding[37–40]. To study whether this mechanism explains mechanotransduction of the E-cadherin/N-cadherin junction we used CRISPR/Cas9 to knock out α-catenin in A431 cells (A431-αcatKO) and expressed α-catenin lacking the vinculin-binding site (A431-αcatΔVBS) or wild-type α-catenin (A431-αcatWT, rescue control). Experiments using either E-cadherin beads (Fig. 4j) or N-cadherin beads (Fig. 4k) showed that reinforcement responses were abrogated in cells lacking α-catenin or its vinculin-binding site. Thus, mechanosensing by E-cadherin/N-cadherin junctions is enabled by vinculin binding to α-catenin. To test whether junctional reinforcement by vinculin binding influenced CAF–A431 interfacial dynamics, we compared heterotypic contact time between CAFs and A431-αcatWT or A431-αcatΔVBS. These experiments showed that impeding vinculin binding to α-catenin shortens contact time significantly, thus indicating that mechanosensing plays a central role in determining junctional integrity (Fig. 4l).

E-cadherin is required for force transmission between A431 cells and CAFs

The fact that the E-cadherin/N-cadherin junction is mechanically active and able to withstand forces does not demonstrate that this junction is responsible for force transmission during CAF-led migration of A431 cells. To address this issue quantitatively, we measured force transmission between CAFs and A431 cells in the presence or absence of E-cadherin (Fig. 5). During contact, control CAFs exerted a force of ∼100 nN on A431 cells, comparable to the force across homotypic junctions in epithelial doublets and sheets[17,18,27,30] (Fig. 5a). When E-cadherin was knocked out in A431 cells, force transmission levels fell dramatically compared with the control case (Fig. 5a), indicating a key role for E-cadherin in force transmission between the two cell types.

We next analysed the time course of force transmission during collective cell migration. Forces between CAFs and control A431 cells exhibited large fluctuations (Fig. 5b–e and Supplementary Video 10), consistent with the dynamic activity of cell–cell adhesion proteins at the CAF–A431 contact (Supplementary Video 7). When CAFs eventually detached from the A431 cells and migrated in isolation, local balance of traction forces within the CAFs was re-established and force transmission between cells vanished (Fig. 5b–e and Supplementary Video 10). In contrast with control A431 cells, force transmission during physical contact between CAFs and A431-EcadKO cells was minimal (Fig. 5b,f–h and Supplementary Video 11). Taken together, our results show that heterotypic adhesions between CAFs and cancer cells transmit tugging forces of similar magnitude to those exerted between homotypic cell doublets and within epithelial monolayers[17,18,27,30].

Impairment of the E-cadherin/N-cadherin junction alters cell migration patterns in two dimensions

We next sought to analyse the cooperative migration of CAFs and A431 cells in 2D spheroid assays. The majority of CAFs are directly followed by cancer cells; we termed these CAFs 'leaders' (Fig. 6a,b and Supplementary Video 12). CAFs that migrated away from the spheroid as isolated cells were called 'loners' (Fig. 6a,b and Supplementary Video 12). The fraction of leaders in CAFs was ∼3-fold higher than that in normal dermal fibroblasts (Fig. 6b, see Supplementary Fig. 4o,p for characterization of normal fibroblasts and CAFs). Similarly, the fraction of leaders in a population of primary lung CAFs was ∼4-fold higher than in fibroblasts obtained from tumour-free parenchyma in the same patients (Fig. 6c). This evidence indicates that the ability of fibroblasts to lead cancer cells correlates with their activation state.

We probed the role of the heterophilic E-cadherin/N-cadherin interaction in determining the fraction of leader versus follower CAFs by using either A431-EcadKO cells or CAF-siNcad. When E-cadherin was knocked out, the percentage of leaders dropped dramatically (Fig. 6d and Supplementary Video 13). N-cadherin siRNA in CAFs also decreased the number of leaders significantly (Fig. 6d). These findings cannot be attributed to an effect of the depletion on the migratory behaviour of each individual cell type because A431-EcadKO spheroids (without CAFs) exhibited the same expansion velocity and shape as their control counterparts (Supplementary Fig. 4e), and CAF-siNcad in isolation migrated at the same velocity as control CAFs (Supplementary Fig. 4n). Taken together, these findings support that the heterophilic E-cadherin/N-cadherin junction is responsible for the guidance of A431 cells by CAFs in 2D migration assays.

N-cadherin, afadin and mechanotransduction are required for CAF repolarization

We next studied whether E-cadherin/N-cadherin junctions are also responsible for the repolarization of CAFs on contact with A431 cells. While CAFs depleted for N-cadherin approached the spheroid with a similar incident angle as controls (Fig. 6e), they did not reverse their polarity, but moved along the spheroid's tangent rather than perpendicularly to it (Fig. 6f and Supplementary Video 13). Removal of E-cadherin also reduced the efficiency of CAF repolarization, albeit to a lesser extent than N-cadherin depletion (Fig. 6f). These observations indicate that N-cadherin plays a role in the guidance of cancer cell migration by CAFs heterophilic adhesions. Further, experiments using A431-αcatΔVBS cells and their rescue control A431-αcatWT demonstrated that junctional mechanotransduction is critical for CAFs to lead A431 migration (Fig. 6g–i).

The lesser effect of E-cadherin knockout on CAF repolarization suggested that other signalling modules may be engaged at the A431/CAF interface. Therefore, we analysed the localization of nectins, their actin-binding partner protein afadin, and cadherin-11, which have previously been implicated in modulating adherens junctions and CIL[16,41] (Fig. 7 and Supplementary Fig. 6). Cadherin-11 did not localize to heterotypic contact zones and depletion

experiments revealed no effect on the ability of CAFs to lead A431 migration (Supplementary Fig. 6a–c). In contrast, nectin-2, nectin-3 and afadin localized at heterotypic contacts (Fig. 7a). Afadin was also localized at the interface between SCC cells and the stroma in patient samples (Supplementary Fig. 7b). Depletion of afadin in CAFs led to a >2-fold decrease in the fraction of leaders and perturbed CAF repolarization following contact with cancer cells (Fig. 7c–f). Thus, the nectin–afadin system is required for both leader/follower patterns of 2D migration and CAF repolarization.

The E-cadherin/N-cadherin junction is required for A431 invasion

We next turned to 3D invasion assays; control spheroids of CAFs mixed with A431 cells invaded the ECM forming multicellular strands led by CAFs (Fig. 8a,f). Strikingly, E-cadherin knockout in A431 cells greatly reduced cancer cell invasion; CAFs invaded the ECM but A431 cells were unable to follow them and remained cohesive in the spheroid (Fig. 8b,f). P-cadherin knockout in A431 cells did not affect invasion (Fig. 8f and Supplementary Fig. 7c). To exclude the possibility that A431-EcadKO cells are generally defective at invasion, we generated spheroids containing a mixture of A431-control cells, A431-EcadKO cells, and CAFs (Fig. 8c). In these experiments, A431-EcadKO cells were observed invading behind wild-type A431 cells (example marked with white arrow in Fig. 8c), but almost never directly behind a CAF. Thus, A431-EcadKO cells are not generically defective at invasion; they are simply defective at following fibroblasts. Consistent with this observation, in 96% of invading strands the cell immediately following the CAFs was a control cell rather than an A431-EcadKO cell (Fig. 8c,g). Knockdown of N-cadherin in CAFs reduced the number of CAF-led invading A431 strands to a similar degree as knockout of E-cadherin in A431 cells (Fig. 8d,f), thus confirming the critical role of heterophilic E-cadherin/N-cadherin adhesion.

The continued cohesion of A431-EcadKO spheroids was unexpected as several studies have reported reduced cohesion and increased single-cell migration following E-cadherin down-regulation[42,43]. We therefore investigated whether the compensatory increase in P-cadherin in A431-EcadKO cells was responsible for cohesion (Supplementary Fig. 4a). We generated A431 cells lacking both E-cadherin and P-cadherin (A431-EPcadKO). When tested in spheroid assays with CAFs, A431-EPcadKO cells could invade as single cells and as cell strands lacking CAFs (Supplementary Fig. 7b,d). Finally, we tested whether junctional mechanotransduction was required for CAFs to lead cancer cell invasion. The number of invasion strands led by CAFs in 3D invasion assays of A431-αcatΔVBS spheroids decreased sharply (Fig. 8e,f). Taken together, this analysis indicates that A431 cells can display a broad repertoire of invasion modes depending on their homotypic adhesion, their heterotypic adhesion with CAFs, and their ability to actively respond to intercellular force. It emphasizes that forces applied on mechanically active E-cadherin/N-cadherin cancer cell–CAF contacts are critical to overcome the cohesive forces exerted by homotypic contacts between E-cadherin-expressing cancer cells that can restrict migration.

DISCUSSION

Cancer progression is increasingly attributed to the aberrant interaction between cancer cells and their microenvironment[44–46]. Non-malignant cell types within this microenvironment can be co-opted by cancer cells to perform functions that are otherwise poorly efficient or altogether unavailable to the tumour[47–49]. While biochemical communication between the tumour and the stroma by growth factors and chemokines (for example, TGFβ, HGF, EGF, CXCL12, CCL7)[10–14] is well established, we identified a physical cooperative invasion mechanism involving a pulling force exerted by CAFs on cancer cells. Force transmission is mediated by a heterophilic junction between E-cadherin expressed by cancer cells and N-cadherin expressed by CAFs. Several studies have demonstrated heterophilic junctions between distinct cadherin pairs[50–55], and recent structural analysis indicates that the heterophilic E-cadherin/N-cadherin interaction has higher binding affinity than the homophilic E-cadherin/E-cadherin one[33]. Consistent with our data, the high-affinity binding in this interaction was dependent on the formation of strand-swap dimers[33]. However, the role of the interaction between E-cadherin and N-cadherin in physiology and disease is virtually unexplored. This gap of knowledge might be attributable, in part, to the traditional notion that expression of distinct cadherins by adjacent tissues favours tissue segregation rather than adhesion[56]. Here we demonstrated that, rather than mediating cell separation, an E-cadherin/N-cadherin interaction enables cancer cell adhesion, migration and invasion. In contrast, we found no evidence of P-cadherin/N-cadherin junctions. Importantly, our analysis establishes that heterotypic junctions not only transmit forces, but also trigger mechanotransduction pathways. This finding raises the possibility that, similarly to the case of homotypic junctions[57], E-cadherin/N-cadherin junctions regulate signalling pathways downstream of a physical force. In this connection, an E-cadherin/N-cadherin junction between cancer cells and osteogenic cells was observed to promote Akt signalling[55], although it was not linked to the application of physical force. A similar role to heterophilic E-cadherin/N-cadherin contacts may be fulfilled by homophilic N-cadherin junctions in tumour cells that have gained N-cadherin expression (Supplementary Fig. 8a). Future work should address the prevalence of heterotypic E-cadherin/N-cadherin adhesions *in vivo*, and study mechanotransduction pathways downstream of this interaction.

Besides enabling adhesion, force transmission and invasion, the heterotypic junction also triggered repolarization of the CAFs favouring their migration away from the spheroid. Repolarization away from a cell–cell contact was first reported in the late 1950s and it is commonly termed CIL[23,24,58,59]. CIL involves transient force transmission through homophilic N-cadherin junctions, followed by cell repolarization, junction dissociation and cell repulsion[23,60]. In contrast with the case of N-cadherin, force transmission through homophilic E-cadherin junctions mediates adhesion but does not trigger CIL[25]. Our observations show that the E-cadherin/N-cadherin junction exhibits features of both E-cadherin and N-cadherin homophilic junctions. Similarly to N-cadherin homophilic junctions, the E-cadherin/N-cadherin junction mediates repolarization so as to create a leading edge on the opposite side of the cell–cell contact. Unlike short-lived N-cadherin homophilic junctions between fibroblasts, the E-cadherin/N-cadherin junction is not disrupted by force application and it enables cells to migrate collectively for several hours. Thus, unlike classical CIL, our results unveil a mechanism in which the asymmetric expression of different cadherins enables cells

to retain adhesion while controlling front/rear polarization of the leading cell. This dual mechanism of ongoing repulsion of CAFs by cancer cells and physical coupling of the cancer cells to the CAFs can explain the persistent and collective outward migration of fibroblasts and cancer cells (Supplementary Fig. 8b—yellow arrows indicate directional guidance and white arrows with borders indicate points of force transmission).

FIB-SEM analysis of heterotypic contact zones revealed a complex interface between cancer cells and CAFs, possibly suggesting a diversity of molecular interactions between the two cell types. It is likely that contact-mediated interactions at the cancer cell–CAF interface trigger numerous changes in cell signalling; indeed, Eph–ephrin signalling has been reported following heterotypic tumour–stroma contact[15]. We also observed nectins and afadin at heterotypic contact sites and afadin depletion prevented CAF repolarization.

Our finding that impairing the E-cadherin/N-cadherin interaction abrogates cancer cell invasion highlights the potential of targeting this interaction to interfere with the dissemination of cancers that metastasize while retaining epithelial characteristics. The absence of such junctions in normal tissue where E-cadherin- and N-cadherin-expressing cells are separated by a basement membrane makes its targeting particularly appealing. While it may be problematic to disrupt E-cadherin or N-cadherin, the nectin/afadin axis may represent a relatively specific target. To conclude, we show that a physical force applied through a heterophilic E-cadherin/N-cadherin junction enables the cooperative invasion of CAFs and cancer cells through a double mechanism: CAFs favour invasion of cancer cells by pulling them away from the tumour, while cancer cells further enhance their spread by polarizing CAF migration away from the tumour. □

METHODS

Methods, including statements of data availability and any associated accession codes and references, are available in the online version of this paper.

Note: Supplementary Information is available in the online version of the paper

ACKNOWLEDGEMENTS

We thank N. Castro for technical assistance, J. de Rooij (UMC Utrecht, Netherlands) for plasmids, S. Pérez-Amodio (IBEC, Spain) for dermal fibroblasts, N. Reguart (Hospital Clinic, Spain) and M. Gabasa (University of Barcelona, Spain) for lung fibroblasts, and A. Schertel (Zeiss) for assistance with the FIB-SEM. This work was supported by the Spanish Ministry of Economy and Competitiveness/FEDER (BFU2012-38146 to X.T., BFU2014-52586-REDT to P.R.-C., IJCI2014-19843 to A.L. and IJCI-2014-19156 to A.E.-A.), the Generalitat de Catalunya (2014-SGR-927 to X.T. and CERCA Programme), the European Research Council (StG-CoG-616480 to X.T.), Obra Social 'La Caixa', Marie-Curie action (CAFFORCE 328664 to A.L.), EMBO Long-term fellowship (EMBO ALTF 1235-2012 to A.L.), a Career Integration Grant within the seventh European Community Framework Programme (PCIG10-GA-2011-303848 to P.R.-C.), Fundació la Marató de TV3 (project 20133330 to P.R.-C.), and AXA research fund (L.A.). E.S., E.A., A.W. and S.D. are funded by the Francis Crick Institute, which receives its core funding from Cancer Research UK (FC001144), the UK Medical Research Council (FC001144), and the Wellcome Trust (FC001144). T.K. is funded by Marie-Curie action (HeteroCancerInvasion no. 708651) and the Japanese Strategic Young Researcher Overseas Visits Program for Accelerating Brain Circulation.

AUTHOR CONTRIBUTIONS

A.L., E.S. and X.T. conceived the study and designed experiments, with additional input from T.K. A.L. performed most experiments and data analysis. T.K. performed and analysed spheroid invasion experiments and generated A431 KO cell lines. A.L., A.E.-A., V.G.-T. and P.R.-C. designed, performed and analysed magnetic cytometry assays. A.B. and X.S.-P. developed software for image analysis and force measurements. S.D. performed QRT–PCR experiments. A.L. and L.A. performed STORM imaging. J.A. contributed CAFs from patients with non-small lung cell carcinoma. E.A. performed the intravital imaging and assisted with the patient sample analysis, A.W. performed electron microscopy. A.L., E.S. and X.T. wrote the manuscript with input from all authors.

COMPETING FINANCIAL INTERESTS

The authors declare no competing financial interests.

Published online at http://dx.doi.org/10.1038/ncb3478
Reprints and permissions information is available online at www.nature.com/reprints

1. Cheung, K. J., Gabrielson, E., Werb, Z. & Ewald, A. J. Collective invasion in breast cancer requires a conserved basal epithelial program. *Cell* **155,** 1639–1651 (2013).
2. Friedl, P., Locker, J., Sahai, E. & Segall, J. E. Classifying collective cancer cell invasion. *Nat. Cell Biol.* **14,** 777–783 (2012).
3. Fischer, K. R. Epithelial-to-mesenchymal transition is not required for lung metastasis but contributes to chemoresistance. *Nature* **527,** 472–476 (2015).
4. Zheng, X. *et al.* Epithelial-to-mesenchymal transition is dispensable for metastasis but induces chemoresistance in pancreatic cancer. *Nature* **36,** 1453–1463 (2015).
5. Gaggioli, C. *et al.* Fibroblast-led collective invasion of carcinoma cells with differing roles for RhoGTPases in leading and following cells. *Nat. Cell Biol.* **9,** 1392–1400 (2007).
6. Harney, A. S. *et al.* Real-time imaging reveals local, transient vascular permeability, and tumor cell intravasation stimulated by TIE2hi macrophage-derived VEGFA. *Cancer Discov.* **5,** 932–943 (2015).
7. Kalluri, R. & Zeisberg, M. Fibroblasts in cancer. *Nat. Rev. Cancer* **6,** 392–401 (2006).
8. Olumi, A. F. Carcinoma-associated fibroblasts direct tumor progression of initiated human prostatic epithelium. *Cancer Res.* **59,** 5002–5011 (1999).
9. Conklin, M. W. & Keely, P. J. Why the stroma matters in breast cancer: insights into breast cancer patient outcomes through the examination of stromal biomarkers. *Cell Adhes. Migr.* **6,** 249–260 (2012).
10. Allinen, M. *et al.* Molecular characterization of the tumor microenvironment in breast cancer. *Cancer Cell* **6,** 17–32 (2004).
11. Oh, E.-Y. *et al.* Extensive rewiring of epithelial-stromal co-expression networks in breast cancer. *Genome Biol.* **16,** 128 (2015).
12. Orimo, A. *et al.* Stromal fibroblasts present in invasive human breast carcinomas promote tumor growth and angiogenesis through elevated SDF-1/CXCL12 secretion. *Cell* **121,** 335–348 (2005).
13. Pietras, K., Pahler, J., Bergers, G. & Hanahan, D. Functions of paracrine PDGF signaling in the proangiogenic tumor stroma revealed by pharmacological targeting. *PLoS Med.* **5,** e19 (2008).
14. Räsänen, K. & Vaheri, A. Activation of fibroblasts in cancer stroma. *Exp. Cell Res.* **316,** 2713–2722 (2010).
15. Astin, J. W. *et al.* Competition amongst Eph receptors regulates contact inhibition of locomotion and invasiveness in prostate cancer cells. *Nat. Cell Biol.* **12,** 1194–1204 (2010).
16. Takai, Y., Miyoshi, J., Ikeda, W. & Ogita, H. Nectins and nectin-like molecules: roles in contact inhibition of cell movement and proliferation. *Nat. Rev. Mol. Cell Biol.* **9,** 603–615 (2008).
17. Liu, Z. *et al.* Mechanical tugging force regulates the size of cell–cell junctions. *Proc. Natl Acad. Sci. USA* **107,** 9944–9949 (2010).
18. Ng, M. R., Besser, A., Brugge, J. S. & Danuser, G. Mapping the dynamics of force transduction at cell–cell junctions of epithelial clusters. *eLife* **3,** e03282 (2014).
19. Bazellières, E. *et al.* Control of cell–cell forces and collective cell dynamics by the intercellular adhesome. *Nat. Cell Biol.* **17,** 409–420 (2015).
20. Buckley, C. D. *et al.* Cell adhesion. The minimal cadherin-catenin complex binds to actin filaments under force. *Science* **346,** 1254211 (2014).
21. Barry, A. K. *et al.* α-catenin cytomechanics–role in cadherin-dependent adhesion and mechanotransduction. *J. Cell Sci.* **127,** 1779–1791 (2014).
22. Abercrombie, M. Contact inhibition and malignancy. *Nature* **281,** 259–262 (1979).
23. Davis, J. R. Inter-cellular forces orchestrate contact inhibition of locomotion. *Cell* **161,** 361–373 (2015).
24. Huttenlocher, A. *et al.* Integrin and cadherin synergy regulates contact inhibition of migration and motile activity. *J. Cell Biol.* **141,** 515–526 (1998).
25. Scarpa, E. *et al.* Cadherin switch during EMT in neural crest cells leads to contact inhibition of locomotion via repolarization of forces. *Dev. Cell* **34,** 421–434 (2015).
26. Tanaka, M., Kuriyama, S. & Aiba, N. Nm23-H1 regulates contact inhibition of locomotion, which is affected by ephrin-B1. *J. Cell Sci.* **125,** 4343–4353 (2012).
27. Maruthamuthu, V., Sabass, B., Schwarz, U. S. & Gardel, M. L. Cell-ECM traction force modulates endogenous tension at cell–cell contacts. *Proc. Natl Acad. Sci. USA* **108,** 4708–4713 (2011).
28. Tambe, D. T. *et al.* Collective cell guidance by cooperative intercellular forces. *Nat. Mater.* **10,** 469–475 (2011).
29. Trepat, X. *et al.* Physical forces during collective cell migration. *Nat. Phys.* **5,** 426–430 (2009).
30. Vedula, S. R. K. *et al.* Epithelial bridges maintain tissue integrity during collective cell migration. *Nat. Mater.* **13,** 87–96 (2014).
31. Nieman, M. T., Kim, J. B., Johnson, K. R. & Wheelock, M. J. Mechanism of extracellular domain-deleted dominant negative cadherins. *J. Cell Sci.* **112,** 1621–1632 (1999).

32. Katsamba, P. *et al.* Linking molecular affinity and cellular specificity in cadherin-mediated adhesion. *Proc. Natl Acad. Sci. USA* **106,** 11594–11599 (2009).
33. Vendome, J. *et al.* Structural and energetic determinants of adhesive binding specificity in type I cadherins. *Proc. Natl Acad. Sci. USA* **111,** E4175–E4184 (2014).
34. Thomson, S. *et al.* Epithelial to mesenchymal transition is a determinant of sensitivity of non-small-cell lung carcinoma cell lines and xenografts to epidermal growth factor receptor inhibition. *Cancer Res.* **65,** 9455–9462 (2005).
35. Tabdili, H. *et al.* Cadherin-dependent mechanotransduction depends on ligand identity but not affinity. *J. Cell Sci.* **125,** 4362–4371 (2012).
36. Weber, G. F., Bjerke, M. A. & DeSimone, D. W. A mechanoresponsive cadherin-keratin complex directs polarized protrusive behavior and collective cell migration. *Dev. Cell* **22,** 104–115 (2012).
37. Le Duc, Q. *et al.* Vinculin potentiates E-cadherin mechanosensing and is recruited to actin-anchored sites within adherens junctions in a myosin II-dependent manner. *J. Cell Biol.* **189,** 1107–1115 (2010).
38. Yonemura, S., Wada, Y., Watanabe, T., Nagafuchi, A. & Shibata, M. α-catenin as a tension transducer that induces adherens junction development. *Nat. Cell Biol.* **12,** 533–542 (2010).
39. Huveneers, S. *et al.* Vinculin associates with endothelial VE-cadherin junctions to control force-dependent remodeling. *J. Cell Biol.* **196,** 641–652 (2012).
40. Twiss, F. Vinculin-dependent cadherin mechanosensing regulates efficient epithelial barrier formation. *Biol. Open* **1,** 1128–1140 (2012).
41. Ikeda, W. *et al.* Tage4/Nectin-like molecule-5 heterophilically trans-interacts with cell adhesion molecule Nectin-3 and enhances cell migration. *J. Biol. Chem.* **278,** 28167–28172 (2003).
42. Perl, A.-K., Wilgenbus, P., Dahl, U., Semb, H. & Christofori, G. A causal role for E-cadherin in the transition from adenoma to carcinoma. *Nature* **392,** 190–193 (1998).
43. Vleminckx, K., Vakaet, L., Mareel, M., Fiers, W. & Van Roy, F. Genetic manipulation of E-cadherin expression by epithelial tumor cells reveals an invasion suppressor role. *Cell* **66,** 107–119 (1991).
44. Egeblad, M., Nakasone, E. S. & Werb, Z. Tumors as organs: complex tissues that interface with the entire organism. *Dev. Cell* **18,** 884–901 (2010).
45. McMillin, D. W., Negri, J. M. & Mitsiades, C. S. The role of tumour–stromal interactions in modifying drug response: challenges and opportunities. *Nat. Rev. Drug Discov.* **12,** 217–228 (2013).
46. Mueller, M. M. & Fusenig, N. E. Friends or foes—bipolar effects of the tumour stroma in cancer. *Nat. Rev. Cancer* **4,** 839–849 (2004).
47. Condeelis, J. & Pollard, J. W. Macrophages: obligate partners for tumor cell migration, invasion, and metastasis. *Cell* **124,** 263–266 (2006).
48. Erez, N., Truitt, M., Olson, P., Arron, S. T. & Hanahan, D. Cancer-associated fibroblasts are activated in incipient neoplasia to orchestrate tumor-promoting inflammation in an NF-κB-dependent manner. *Cancer Cell* **17,** 135–147 (2010).
49. Hanahan, D. & Coussens, L. M. Accessories to the crime: functions of cells recruited to the tumor microenvironment. *Cancer Cell* **21,** 309–322 (2012).
50. Apostolopoulou, M. & Ligon, L. Cadherin-23 mediates heterotypic cell–cell adhesion between breast cancer epithelial cells and fibroblasts. *PLoS ONE* **7,** e33289 (2012).
51. Omelchenko, T. *et al.* Contact interactions between epitheliocytes and fibroblasts: formation of heterotypic cadherin-containing adhesion sites is accompanied by local cytoskeletal reorganization. *Proc. Natl Acad. Sci. USA* **98,** 8632–8637 (2001).
52. Ounkomol, C., Yamada, S. & Heinrich, V. Single-cell adhesion tests against functionalized microspheres arrayed on AFM cantilevers confirm heterophilic E- and N-cadherin binding. *Biophys. J.* **99,** L100–L102 (2010).
53. Straub, B. K. *et al.* E-N-cadherin heterodimers define novel adherens junctions connecting endoderm-derived cells. *J. Cell Biol.* **195,** 873–887 (2011).
54. Volk, T., Cohen, O. & Geiger, B. Formation of heterotypic adherens-type junctions between L-CAM-containing liver cells and A-CAM-containing lens cells. *Cell* **50,** 987–994 (1987).
55. Wang, H. *et al.* The osteogenic niche promotes early-stage bone colonization of disseminated breast cancer cells. *Cancer Cell* **27,** 193–210 (2015).
56. Fagotto, F. The cellular basis of tissue separation. *Development* **141,** 3303–3318 (2014).
57. Benham-Pyle, B. W., Pruitt, B. L. & Nelson, W. J. Cell adhesion. Mechanical strain induces E-cadherin-dependent Yap1 and β-catenin activation to drive cell cycle entry. *Science* **348,** 1024–1027 (2015).
58. Abercrombie, M. & Heaysman, J. E. Observations on the social behaviour of cells in tissue culture. I. Speed of movement of chick heart fibroblasts in relation to their mutual contacts. *Exp. Cell Res.* **5,** 111–131 (1953).
59. Carmona-Fontaine, C. *et al.* Contact inhibition of locomotion *in vivo* controls neural crest directional migration. *Nature* **456,** 957–961 (2008).
60. Theveneau, E. *et al.* Chase-and-run between adjacent cell populations promotes directional collective migration. *Nat. Cell Biol.* **15,** 763–772 (2013).

DOI: 10.1038/ncb3478

METHODS

Cell culture. Human vulval CAFs[61] were isolated from patient tissue samples and immortalized by pBABE-Hygro-HTERT retroviral transfection. Stably labelled CAFs were obtained by using a lentiviral CAGAP-mCherry construct. CAFs were cultured in DMEM supplemented with 10% FCS and 1% insulin–transferrin–selenium (Invitrogen, no. 41400-045) and 100 U ml^{-1} penicillin, 100 µg ml^{-1} streptomycin. A431 is a human epidermoid carcinoma cell line described in the ATCC collection. A431 cells were grown in DMEM supplemented with 10% FCS, 100 U ml^{-1} penicillin, 100 µg ml^{-1} streptomycin. Primary human lung fibroblasts from three adenocarcinoma patients were cultured as previously described[62,63] in DMEM-based culture medium supplemented with 10% FBS. Lung CAFs were obtained with informed patient consent and with the approval of the Ethics Committees of the Universitat de Barcelona and the Hospital Clínic. Three days before experiments, lung CAFs and lung normal fibroblasts were pre-activated with 2.5 ng ml^{-1} of TGF-β1 (R&D Systems) to render a phenotype similar to that found *in vivo*[62]. H1437 cells were grown in RPMI supplemented with 10% FCS, 100 U ml^{-1} penicillin, 100 µg ml^{-1} streptomycin. VSCC4 and VCAF4 were isolated from a vulval squamous cell carcinoma patient following Research Ethics Committee approval 15/EE/0151 and OCAF2 were isolated from an oral squamous cell carcinoma patient following Research Ethics Committee approval CCR 2924 (St Mary's REC). FaDu cells are a pharynx SCC cell line described in the ATCC collection. Cell lines used in this study are not listed in the database of commonly misidentified cell lines maintained by ICLAC, and they were not authenticated. Cell lines were tested for mycoplasma contamination.

Stable cell lines. E-cadherin, P-cadherin, E-/P-cadherin double, and α-catenin CRISPR–Cas9 A431 cells were generated as follows. Gene-specific guide RNA (gRNA) and Cas9 expression vectors were purchased from Santa Cruz Biotechnology or constructed by designing gRNA using a gRNA designing tool (F. Zhang's laboratory, MIT, USA). Plasmids with different gRNA sequences targeting E-cadherin, P-cadherin or α-catenin were transfected together into A431 cells using Xtremegene HP DNA transfection reagent (Roche) according to the manufacturer's recommendation. At 48 h after transfection, GFP-positive cells were sorted by FACS into 96-well plates for single-colony isolation. Target-gene-deleted clones were screened by western blot with E-cadherin, P-cadherin or α-catenin antibody, and insertion/deletion (InDel) of the target sites was analysed by sequencing of genomic DNA using the following primers: E-cadherin sequence 1 forward: GCTCTGAGGAGTGGTGCATT, E-cadherin sequence 1 reverse: GATCCCCAAATCTGCGTAAA, E-cad sequence 2 forward: ACTGTGCCCA GTCGAGAAGT, E-cadherin sequence 2 reverse: GATTCAGTCCCAGACG GTGT, P-cadherin sequence 1: CCTCGTGGCGCTGGACCAAT, α-catenin sequence1: CTGTGTAACAAGAGGCTCCAA .

E-cad-Ruby-WT- or E-cad-Ruby-W2A-expressing plasmids were transfected into A431-EcadKO cells using Lipofectamine 2000 according to the manufacturer's recommendation. Forty-eight hours after transfection, cells started to be selected by G418. After 2 weeks of selection, cells with Ruby signal were sorted and collected by FACS.

α-catenin-mCherry-WT or -ΔVBS lentiviral plasmid was transfected into 293FT cells together with plasmids encoding RRE, REV and VSVG using ProFection Mammalian Transfection System-Calcium Phosphate (Promega) according to the manufacturer's recommendation. Medium was changed 24 h after transfection. After another 24 h of incubation, viral supernatant was collected and purified by passing through a 0.4 µm filter, and added to A431-αCatKO cells. Seventy-two hours after transfection, cells started to be selected by puromycin for 2 days. Selected mCherry-positive cells were then sorted and collected by FACS.

To generate CAFs stably expressing N-cadherin-GFP, CAFs were infected with N-cad-GFP-containing lentiviral vector that was produced by transfecting lentiviral plasmid as well as VSVG-, RRE- and REV-encoding plasmids into 293FT cells. Seventy-two hours after infection, CAFs were selected by puromycin. After 2 days of selection, the cells were sorted for GFP and collected by FACS.

Characterization of all stable cell lines can be found in Supplementary Fig. 4.

2D spheroid assay. By using an Ultra Low Attachment 96-well round-bottomed plate (Corning) a cell suspension at concentration of 0.5×10^4 A431 cells per well was cultured in a total volume of 200 µl of complete medium. After 2 days of culture, 500-µm-diameter spheroids were seeded on the fibronectin-coated polyacrylamide gel overnight at 37 °C. After spheroid attachment on the substrate, a suspension of CAFs (0.3×10^4 cells per well) was added. CAFs were then allowed to attach before the beginning of experiments.

siRNA and transfections. CAFs and A431 cells were cultured in standard conditions and transfected using Lipofectamine RNAiMAX Reagent (Life Technologies, no. 13778-075). Cells were plated at 60% confluence and subjected to transfection the following day using 50 picomoles of a pool of 3 siRNAs and used 72 h after transfection. siRNA was purchased from Life Technologies and sequences are listed below: N-cadherin, gene: CDH2, siRNA: no. s2771, no. s2772, no. s2773, sequence 5′-3′: GUGCAACAGUAUACGUUAAtt, GGGUAAUCCUCCCAAAUCAtt, GAACAUAUGUGAUGACCGUtt, siRNA CT negative control siRNA, no: 4390843, afadin, gene: MTTL4, siRNA: no. 144142, no. 144143, no. 144144, sequence 5′-3′: CCUGAUAUGCGAAUGGCUGUtt, GGUGGUUAUGAAACGACGGtt, CCUCU AGUUGUACAACUGAtt, cadherin-11, gene: CDH11 siRNA: no. s2798, no. s2799, no. s2800, sequence 5′-3′: CGACAGAUUUUUCACUAUUtt, CCACCAAAGUU UCCGCAGAtt, GAAUCCUGAUGGUAUCAAUtt . To visualize N-cadherin in CAFs and E-cadherin in A431 cells during time-lapse experiments, unless stated otherwise cells were transfected with the N-cadherin-EGFP plasmid (Addgene, no. 18870) and E-cadherin-Ruby plasmid (from K. Anderson's laboratory, Crick Institute, UK) respectively two days before experiments using the Neon transfection device according to the manufacturer's instructions (Invitrogen).

QRT–PCR. QRT–PCR was used to determine the expression of mRNAs of interest relative to a control mRNA. Platinum SYBR Green qPCR SuperMix-UDG with Rox (Invitrogen) was used in conjunction with a 7900HT Fast Real-Time PCR system (Applied Biosystems). Primer sequences: E-cadherin: forward TCACCACTGGGCT GGACCGA, reverse TACAGCCTCCCACGCTGGGG, P-cadherin: forward TTCC GCTGTAGCCGCAAGGC, reverse GTTGAGGCCCCAGCGAACCC, N-cadherin: forward TCAAACACAGCCACGGCCGT, reverse CGGTCTGGATGGCGAACC GT .

3D invasion assay. A431 and CAF cells were removed from the cell culture dishes with trypsin and re-suspended in sterile 0.25% methylcellulose solution in DMEM. The cellulose solution contained a 1:1 ratio of A431 and CAF cells at a concentration of 1×10^5 cells per millilitre. Twenty-microlitre droplets were plated onto the underside of a 10 cm culture dish and allowed to form spheroids in a 37 °C incubator overnight. The spheroids were then embedded in a collagen I/Matrigel gel mix at a concentration of approximately 4 mg ml^{-1} collagen I and 2 mg ml^{-1} Matrigel (BD Bioscience) in 24-well glass-bottomed cell culture plates (MatTek) on a 37 °C hot block. The gel was incubated for at least 30 min at 37 °C with 5% CO_2. The gel was covered with DMEM media containing 10% FCS. Sixty hours later, the spheroids embedded in the gel were washed with PBS and then fixed for 20 min at room temperature with 4% paraformaldehyde. The spheroids were then imaged with an inverted Zeiss LSM780 at a magnification of ×10, ×20 and ×63. *z* stack images spanning 100–150 µm were collected and image stacks were processed by ZEN software (Carl Zeiss) to yield maximum-intensity projections.

Polyacrylamide gel preparation. Polyacrylamide gels with a Young's modulus of 6 kPa were prepared as described previously[64]. Briefly, a solution of 7.5% acrylamide (Bio-Rad, no. 161-0140), 0.06% bis-acrylamide (Bio-Rad, no. 161-0140) and 1.4% 200-nm-diameter green fluorescent carboxylate-modified beads (Invitrogen, no. F8811) was prepared and polymerized by addition of 0.5% ammonium persulfate and 0.05% tetramethylethylenediamine. The thickness of the polymerized gel was set as approximately 100 µm height by using a 12 µl drop of the polyacrylamide solution covered by a 12 mm glass coverslip. After polymerization, the gel surface was activated with sulfo-SANPAH (Thermo Scientific) and coated with 40 µg ml^{-1} of fibronectin (Sigma, no. F0895) overnight.

Immunostaining. Cells were fixed with 4% paraformaldehyde for 10 min and permeabilized in 0.1% Triton X-100 for 10 min. Cells were blocked in 1% BSA for 1 h before being incubated for 2 h with primary antibodies. After incubation for 2 h with the appropriate fluorescence-conjugated secondary antibodies, cells were washed and mounted in Mowiol reagent. Images were acquired with a Nikon C1Si confocal microscope with a spinning-disc confocal unit (CSU-W1, Yokogawa), a Zyla sCMOS camera (Andor) and a 60× oil immersion objective (NA = 1.42).

Tissue section sample preparation. Human head and neck squamous cell carcinoma samples were collected under ethical approval CCR 2924 (St Mary's REC) and stained as previously described[65]. Briefly, fresh frozen sections were fixed in 4% paraformaldehyde, permeabilized in 0.2% Triton X-100, and stained with the following antibodies: anti-E-cadherin monoclonal antibody (HECD-1 Crick Institute hybridoma cell services), anti-β-catenin (Santa Cruz no. sc7963), anti-p120catenin (BD Biosciences no. 610133), anti-afadin (Atlas Ab no. HPA030212, anti-αSMA (Sigma no. A2547), anti-active integrin β1 (9EG7 BD Pharmingen no. 556048), and anti-fibronectin (dilution 1/500, Sigma no. F3648). Unless stated otherwise, all antibodies were used at 1:100 dilution. Sections were mounted using MOWIOL reagent and imaged using a Zeiss LSM 780.

Antibodies, drugs and reagents. The primary antibodies used were: anti-E-cadherin monoclonal antibody (HECD-1, Crick Institute hybridoma cell services), anti-N-cadherin monoclonal antibodies (clone 014, Sino Biological,

no. 11039-H08H or clone 8C11, Thermo Scientific, no. MA1-2002), anti-P-cadherin monoclonal antibody (clone 6A9, Upstate MerckMillipore, no. 05-916), anti-β-catenin monoclonal antibody (clone 14, BD Transduction Laboratories, no. 610153), anti-β-catenin polyclonal antibody (Thermo Scientific, no. 71-2700), anti-β-catenin monoclonal antibody (Santa Cruz Biotechnology, no. sc7963), anti-cadherin-11 monoclonal antibody (CadherinOB, Thermo Scientific, clone 16A, no. MAI-06306), blocking antibody anti-E-cadherin monoclonal antibody (DECMA-1, Sigma, no. U3254), anti-nectin3 polyclonal antibody (C-19, Santa Cruz Biotechnology, no. sc-14806), anti-nectin2 monoclonal antibody (clone B-C12, abcam, no. ab27344), anti-afadin polyclonal antibody (anti-MLLT4, Sigma, no. HPA030212), anti-alpha-catenin monoclonal antibody (clone (15D9), Enzo Life Science, no. ALX-804-101-C100), anti-vinculin polyclonal antibody (phospho Y821, abcam, no. ab 61071), Alexa Fluor 647 phalloidin (Thermo Fischer Scientific, no. A22287), anti-active beta1 integrin (BD Pharmingen no. 556048), anti-fibronectin (SIGMA, no. F3648) dilution 1:500 for WB, anti-actin (SIGMA, no. a3853), anti-alpha smooth muscle actin (SIGMA, no. A2547). The secondary antibodies used for immunofluorescence were: Alexa Fluor 647 anti-rabbit (Life Technology. no. A-21245) or Alexa Fluor 488 anti-rabbit (Life Technology. no. A-21206), Alexa Fluor 488 anti-mouse (Life Technology. no. A-11029) or Alexa Fluor 555 anti-mouse (Life Technology. no. A-21424) and were diluted 1:400. For immunostainings, unless stated otherwise all primary antibodies were used at 1:200 dilution and secondary antibodies at 1:400.

Western blotting. Protein expression levels were measured using western blotting. Cells were lysed with Laemmli 1× (Sigma) containing 2.5% β-mercaptoethanol (Bio-Rad) and heated at 95 °C for 5 min. Next, cell lysates were loaded to 4–20% polyacrylamide gels (Bio-Rad) for electrophoresis. Proteins were then transferred to a nitrocellulose membrane (Whatman, GE Healthcare Life Sciences), which was blocked with 5% dry milk, Tris buffer saline, 0.2% Tween, and incubated with primary antibodies (overnight at 4° C) followed by horseradish-peroxidase-coupled secondary antibodies (Jackson, no. 715-035-151), for 1 h at room temperature. Bands were revealed using the LumiLight kit (Roche) or with Luminata Classico (EMD Millipore) and bands were detected by ImageQuant LAS4000 (GE Healthcare Life Sciences). Quantification of the band intensity was performed with ImageJ software. The quantified data were normalized to α- or β-tubulin expression and are expressed as the average of three independent experiments (mean ± s.d.); α- or β-tubulin was used as an endogenous loading control. Anti-E-cadherin mouse monoclonal antibody (clone: HECD-1, Crick Institute hybridoma cell services), anti-P-cadherin rabbit polyclonal antibody (cat no. 2130, Cell Signaling Technology), anti-afadin polyclonal antibody (anti-MLLT4, Sigma, no. HPA030212), anti-N-cadherin monoclonal antibodies (clone 014, Sino Biological, no. 11039-H08H or clone 8C11, Thermo Scientific, no. MA1-2002), anti-cadherin-11 monoclonal antibody (CadherinOB, Thermo Scientific, clone 16A, no. MAI-06306), anti-beta tubulin monoclonal antibody (Sigma, no. T7816) 1:2,000 dilution were used. For western blotting, all antibodies were used at 1:1,000 dilution unless state otherwise, and secondary antibodies were used at 1:2,000 dilution.

Magnetocytometry. Bead pulling experiments were performed using magnetic tweezers as previously described[19,66]. Briefly, 4.47-μm-diameter ferromagnetic beads with carboxyl surface groups (Spherotech) were covalently coated with a 32 μg ml^{-1} solution of purified E-cadherin–Fc (Creative Biomart, no. CDH1-274H), P-cadherin–Fc (R&D Systems, no. 861-PC) or N-cadherin–Fc (Creative Biomart, no. CDH2-315H) proteins. Beads were first washed with Na phosphate buffer (0.1 M, pH 8), incubated with 32 μg ml^{-1} of the Fc-tagged proteins for 5 h at 4 °C and then with crosslinking buffer for 1 h (25 mM DMP, 0.2 M triethanolamine, pH 8.2). The protein-coated beads were allowed to settle on a 70% confluent monolayer of cells for 30 min before starting the experiment. To measure the extent of reinforcement, a pulsatory force of 1 Hz and 0.1 nN was applied to beads attached to cells for 4 min. The force exerted by the tweezers was calibrated from the velocity of beads in liquids of known viscosity measured as a function of the tip–bead distance and applied current, as previously described[66,67]. Bead movement in response to the pulsatory force was tracked using a custom-made tracking software. Stiffness of the cell–bead contact was calculated as the ratio between the amplitude of the applied force and that of the observed bead oscillation. The magnetic force generated by the magnet is restricted to the close proximity of the magnet tip[66]. The number of beads probed per cell was limited to two (generally only one). For β-catenin, P-cadherin or E-cadherin recruitment mediated by N-cadherin, magnetic-coated beads were measured using magnetic twisting cytometry as previously described[19,21]. For bead detachment assays, the tip of the magnetic tweezers device was used to apply a constant force of 0.5 nN for 1 min on the beads attached to the cells. Then, the percentage of beads still attached to cells after force application was calculated as previously described[66]. For bead detachment assay with blocking antibody E-cadherin, A431 cells were incubated 2 h with cell media containing 64 μg ml^{-1} (1:500 dilution) DECMA-1 antibody then washed with normal media and incubated with the beads.

Time-lapse acquisition. For 2D spheroid assays, multidimensional acquisitions were performed 30 min after CAFs seeding on the attached spheroid. Fluorescence and bright-field images were obtained every 10 min during at least 10 h. Acquisitions were performed on an automated inverted microscope (Nikon Eclipse Ti, ×10 lens) equipped with thermal, CO_2 and humidity control, using MetaMorph (Universal Imaging) software.

For time-lapse acquisition of mixed CAFs and A431 cells, a ratio of 1:1 of the two cell types was seeded on a glass-bottom well plate and allowed to adhere overnight. The following day, time-lapse imaging was performed. To observe the E-cadherin/N-cadherin dynamics at the spheroid edges, spheroids of A431 cells expressing E-cadherin-Ruby were prepared as described above and seeded overnight on 6-well glass-bottom plates. The following day, a solution of 0.5×10^4 CAFs expressing N-cadherin-GFP was deposited on the glass-bottom well plate containing the attached spheroid. Acquisitions were performed 7 h after CAF seeding. For time-lapse acquisition during EGTA treatment, CAFs stably expressing N-cadherin-GFP were mixed overnight with A431 cells stably expressing E-cadherin-Ruby on glass coverslips (ratio 1:1). After 10 min of acquisition, the EGTA solution was added to the medium (final concentration: 4 mM). After 4 min incubation, the medium containing EGTA was washed three times with normal medium on acquisition. Time-lapse imaging on glass substrate was performed with a Nikon C1Si confocal microscope with a spinning-disc confocal unit (CSU-W1, Yokogawa), a Zyla sCMOS camera (Andor) and a ×60 oil immersion objective (NA = 1.42) or using a ×40 objective, 1.3 NA oil Plan-Apochromat immersion lens on an LSM 710 Zeiss confocal microscope.

Traction force microscopy. Traction forces were computed using Fourier-transform traction microscopy with finite gel thickness as previously described[29]. Force unbalance was computed as the traction integral over the area occupied by the cell. For this purpose, masks were generated based on the CAF fluorescence images. To measure baseline noise, the same procedure was performed on a cell-free region.

Velocity and curvature analysis, contact time duration of the spheroid edge by CAFs. Velocities and curvature were obtained as previously described[29]. CAF trajectories were tracked using the Manual Tracking plug-in from ImageJ. At each time point, CAFs in contact with the spheroid were analysed. For each CAF the mean cell velocity and edge curvature within a range of 40 μm centred in the CAF were computed. This process was repeated on the same number of random positions over the spheroid contour (excluding CAF positions). Quantification of velocity of individual CAFs displayed in Supplementary Fig. 4n,q was performed and analysed using the Manual Tracking and Chemotaxis Tool plug-ins from ImageJ. For quantification of velocity in 3D ECM, CAFs transfected as previously described with siRNA control or siRNA N-cadherin or control A431 cells or A431-EcadKO cells were mixed in 12-well glass-bottom plates with a solution of ECM as previously described to a final density of 3×10^3 cell per gel. Twenty-four hours after polymerization of the gel time-lapse imaging (1 acquisition per 15 min with bright-field imaging) was acquired with a Nikon C1Si confocal microscope with a spinning-disc confocal unit (CSU-W1, Yokogawa), a Zyla sCMOS camera (Andor) and a ×10 objective. Tracking of cells was performed with ImageJ manual tracking plug-in over around 30 slides and cell velocity was calculated as the accumulated distance/total time acquired.

Gel contraction assay. CAFs or normal fibroblasts were mixed with a solution of ECM previously described[5] to a final density of 7×10^4 cells per gel and seeded in 24-well glass-bottom plates. After 1 h of gel polymerization cell culture medium was added to the gels. Measurement of the percentage of contraction of the gel was performed using the Polygon selection function in ImageJ by taking the initial area of the gel as reference (D0, day 0). Gel contraction was then quantified 24 h and 48 h after polymerization (D1 = day 1, D2 = day 2). For each condition, for each independent experiment gels were analysed in triplicate.

Measurement of heterotypic contact time. An amount of 25,000 A431 cells (E-cadherin-Ruby or α-catenin-mCherry) and 30,000 N-cadherin-GFP CAFs were seeded into each side of 2-well culture insert (ibidi) on a glass-bottom dish and cultured for 24 h. Then the insert was removed and complete culture medium was added. Fourteen hours later, the medium was changed to phenol red-free DMEM with 10% FBS and 1% ITS. Time-lapse images of Ruby/mCherry and GFP signals at A431–CAF contact sites were acquired at 5 min intervals using a ×40 objective, 1.3 NA oil Plan-Apochromat immersion lens on an LSM 710 Zeiss confocal microscope. The quantification of lifetime of E-cadherin/N-cadherin contact was based on fluorescent co-localization at A431–CAF interfaces. Three classes of duration time were defined: longer than 60 min (>60), between 30 to 60 min (30–60) and less than 30 min (<30).

Super-resolution optical imaging. For STORM imaging, cells were seeded and immunostained as described above. Images were acquired using a Nikon N-STORM

DOI: 10.1038/ncb3478

4.0 system configured for total internal reflection fluorescence (TIRF) imaging. Excitation inclination was tuned to adjust focus and to maximize the signal-to-noise ratio. Fluorophores were excited illuminating the sample with the 647 nm (~160 mW), and 488 nm (~80 mW) laser lines built into the microscope. Fluorescence was collected by means of a Nikon ×100, 1.4 NA oil immersion objective and passed through a quad-band-pass dichroic filter (97335 Nikon). Images were recorded onto a 256 × 256 pixel region (pixel size 160 nm) of a sCMOS camera (Hamamatsu). Alexa647 and Alexa488 channels were recorded sequentially and absence of cross-talk under these conditions verified. Samples were kept in OxEA buffer for STORM imaging as previously described[68]. Single-molecule localization sequences were analysed with the STORM plug-in of NIS element Nikon software. Structured illumination microscopy was performed using a Zeiss ELYRA system as previously described[69].

Intravital imaging. An amount of 3–5 × 10^5 cells (1:1 mixture of VCAF2B-YPet and A431-mCherry) were injected intradermally in the ear of a Nu/Nu mouse in PBS + 50% Matrigel in a volume of 10 µl with an insulin syringe. At 4 and 7 days post-injection, the animal was anaesthetized (isoflow) for intravital imaging and the ear immobilized with tape to prevent movement artefacts. Imaging was performed using the Inverted Zeiss LSM 780 multiphoton laser scanning confocal microscope in lambda mode with the 561 nm 1P-laser and the 2P-laser at 930 nm followed by spectral unmixing with Zen software.

Mice were female and between 6 and 12 weeks old. Experiments were carried out under Home Office Project Licence 70/8380, which passed ethical review by the LRI Animal Welfare Ethical Review Board in 2014. No statistical method was used to predetermine sample size. The experiments were not randomized. The investigators were not blinded to allocation during experiments and outcome assessment.

Electron microscopy. For transmission electron microscopy, cells were fixed in 4% paraformaldehyde/2.5% glutaraldehyde in 0.1 M phosphate buffer (pH 7.4), followed by incubation in reduced osmium tetroxide for 1 h and then 1% tannic acid in 0.05 M sodium cacodylate for 45 min. Ultrathin sections were cut on a UCT ultramicrotome (Leica Microsystems UK) and stained with lead citrate before being examined in a JEOL 1010 microscope and imaged with a Bioscan CCD (charge-coupled device; Gatan UK). For focused ion beam scanning electron microscopy (FIB-SEM), A431 cells and CAF spheroids were prepared and imaged as described previously[70]. Briefly, a Zeiss NVision 40 FIB-SEM was used to image the volume of interest. The sample was embedded in resin with a heavy metal stain added to provide electron contrast. A focused beam of ions was used to remove thin layers of material from the block face, allowing sequential SEM imaging at 50 nm intervals through the volume.

Statistics and reproducibility. Unless otherwise specified, statistical comparisons were then performed by using parametric *t*-tests or non-parametric Mann–Whitney's test. Unless otherwise specified, all data shown are mean ± s.e.m. Statistical differences between distributions were performed using the Kolmogorov–Smirnov test or Chi square test as indicated in the figure legends. When representative images are shown, these represent at least three samples, apart from Figs 3a–d and 7a where images shown are the representative of two experiments.

Code availability. Computer code used in this study can be made available on request to the corresponding authors.

Data availability. All data supporting the findings of the study are available from the authors on reasonable request.

61. Calvo, F. *et al.* Mechanotransduction and YAP-dependent matrix remodelling is required for the generation and maintenance of cancer-associated fibroblasts. *Nat. Cell Biol.* **15,** 637–646 (2013).
62. Puig, M. *et al.* Matrix stiffening and β1 integrin drive subtype-specific fibroblast accumulation in lung cancer. *Mol. Cancer Res.* **13,** 161–173 (2015).
63. Vizoso, M. *et al.* Aberrant DNA methylation in non-small cell lung cancer-associated fibroblasts. *Carcinogenesis* **36,** 1453–1463 (2015).
64. Serra-Picamal, X. *et al.* Mechanical waves during tissue expansion. *Nat. Phys.* **8,** 628–634 (2012).
65. Hidalgo-Carcedo, C. *et al.* Collective cell migration requires suppression of actomyosin at cell–cell contacts mediated by DDR1 and the cell polarity regulators Par3 and Par6. *Nat. Cell Biol.* **13,** 49–58 (2011).
66. Roca-Cusachs, P., Gauthier, N. C., Del Rio, A. & Sheetz, M. P. Clustering of α(5)β(1) integrins determines adhesion strength whereas α(v)β(3) and talin enable mechanotransduction. *Proc. Natl Acad. Sci. USA* **106,** 16245–16250 (2009).
67. Kollmannsberger, P. & Fabry, B. High-force magnetic tweezers with force feedback for biological applications. *Rev. Sci. Instrum.* **78,** 114301 (2007).
68. Nahidiazar, L. *et al.* Optimizing imaging conditions for demanding multi-color super resolution localization microscopy. *PLoS ONE* **11,** e0158884 (2016).
69. Madsen, C. D. *et al.* STRIPAK components determine mode of cancer cell migration and metastasis. *Nat. Cell Biol.* **17,** 68–80 (2014).
70. Armer, H. E. J. *et al.* Imaging transient blood vessel fusion events in zebrafish by correlative volume electron microscopy. *PLoS ONE* **4,** e7716 (2009).

nature cell biology

DOI: 10.1038/ncb3478

In the format provided by the authors and unedited.

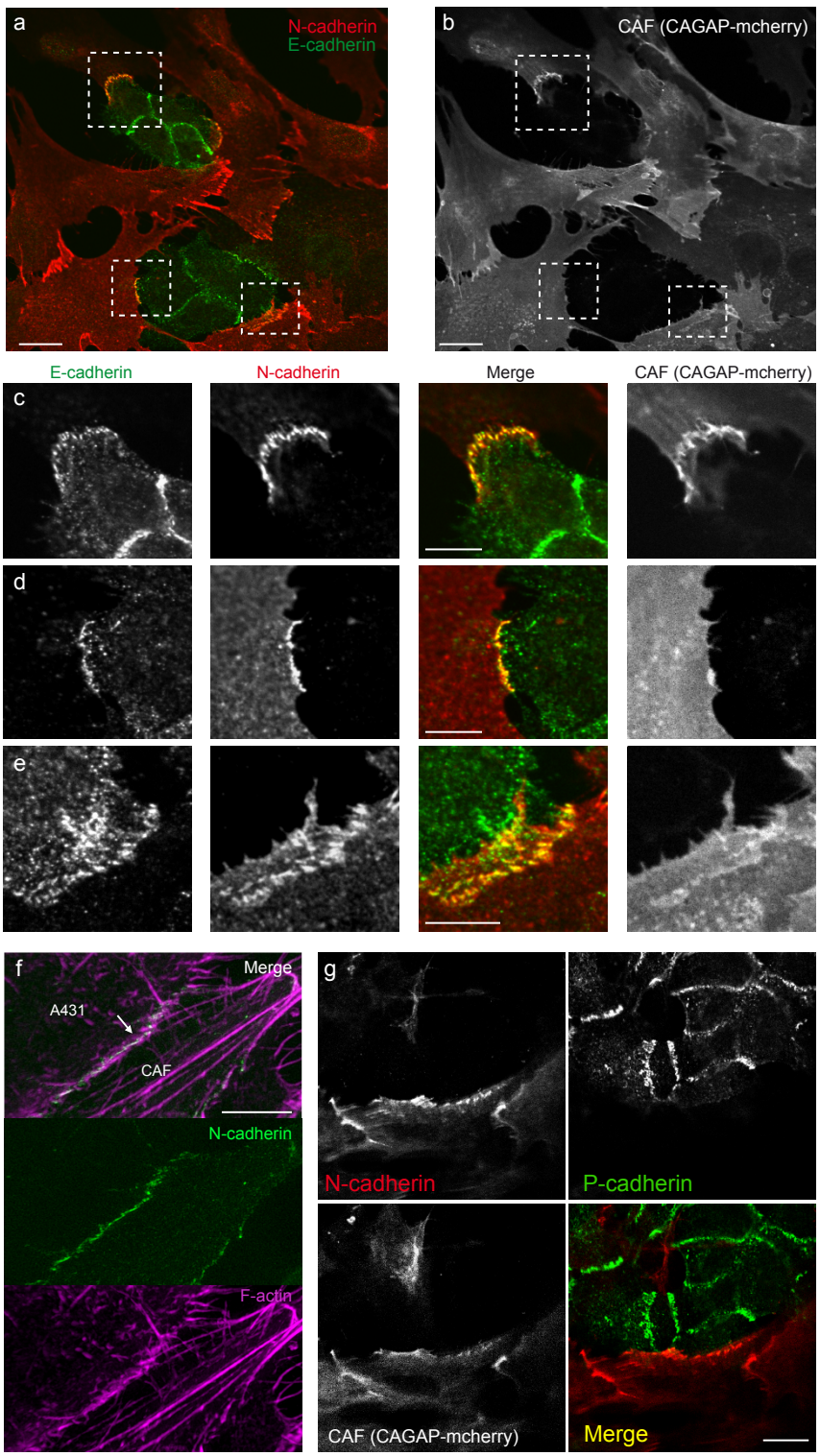

Supplementary Figure 1 CAFs and A431 cells form heterophilic E-cadherin/N-cadherin junctions. **(a,b)** Fluorescence images of a co-culture of CAFs (CAGAP-mcherry) and A431 cells stained for N-cadherin (far-red) and E-cadherin (green). Scale bars, 20µm. **(c-e)** 3 magnified views of the regions highlighted by white rectangles in **a**. Images representative of 3 samples. Scale bars, 10µm. **(f)** SIM immunofluorescence images of A431 cells contacting a CAF, N-cadherin (green), F-actin (magenta). Images representative of 15 samples. Scale bar, 5µm. **(g)** Fluorescence images of a co-culture of CAFs (CAGAP-mcherry) and A431 cells stained for N-cadherin (far-red) and P-cadherin (green). Images representative of 3 samples. Scale bars, 20µm.

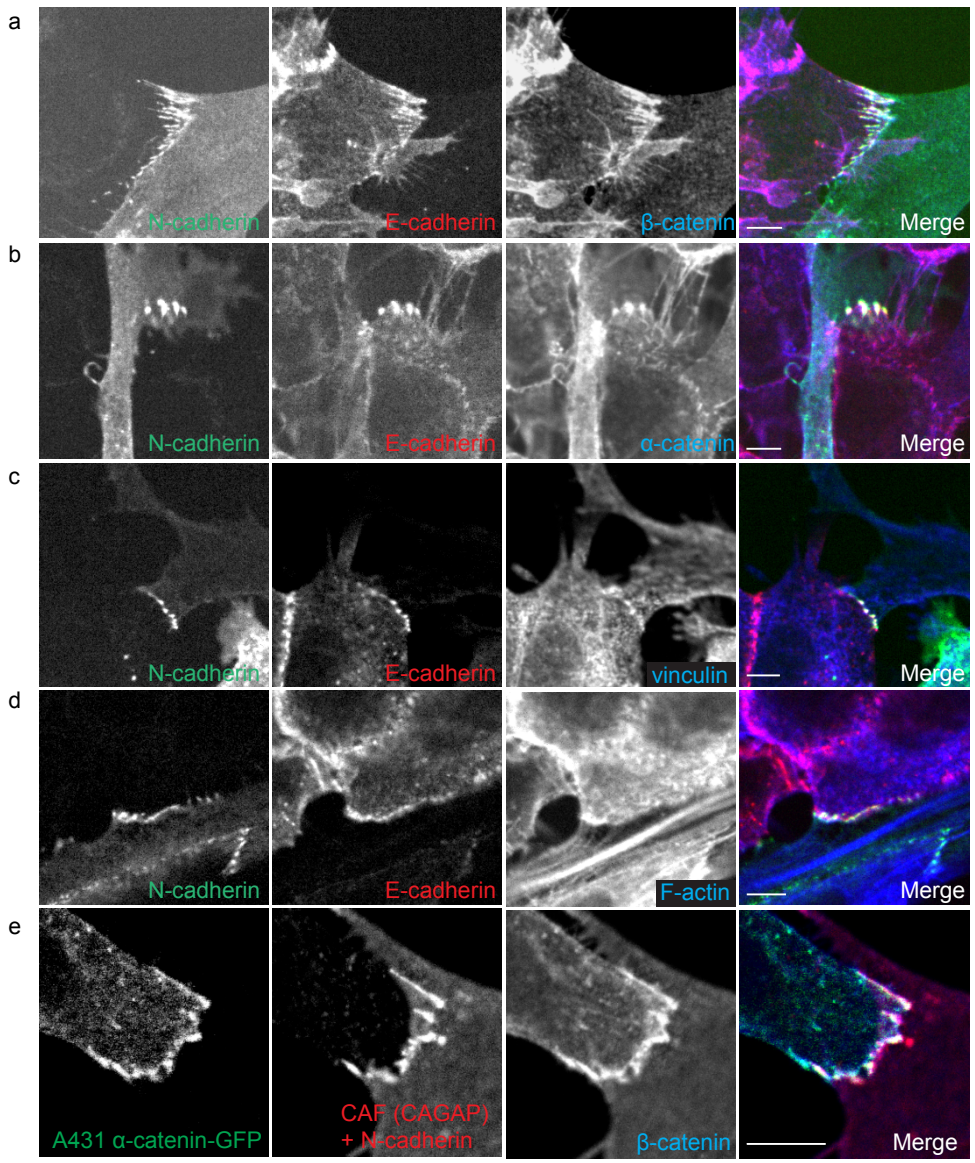

Supplementary Figure 2 Heterophilic E-cadherin/N-cadherin junctions between CAFs and A431 cells colocalize with β-catenin, α-catenin, vinculin, and F-actin. **(a-d)** Fluorescence images of a co-culture of CAFs expressing N-cadherin-GFP and A431 cells expressing E-cadherin-Ruby stained for β-catenin (a), α-catenin (b), vinculin (c), F-actin (far red) (d). Images representative of 3 samples. Scale bars, 5μm. **(e)** Representative fluorescence images of a co-culture of CAFs (CAGAP-mcherry) and A431 cells expressing α-catenin-GFP stained for N-cadherin (red) and β-catenin (blue). Images representative of 2 samples. Scale bars, 5μm.

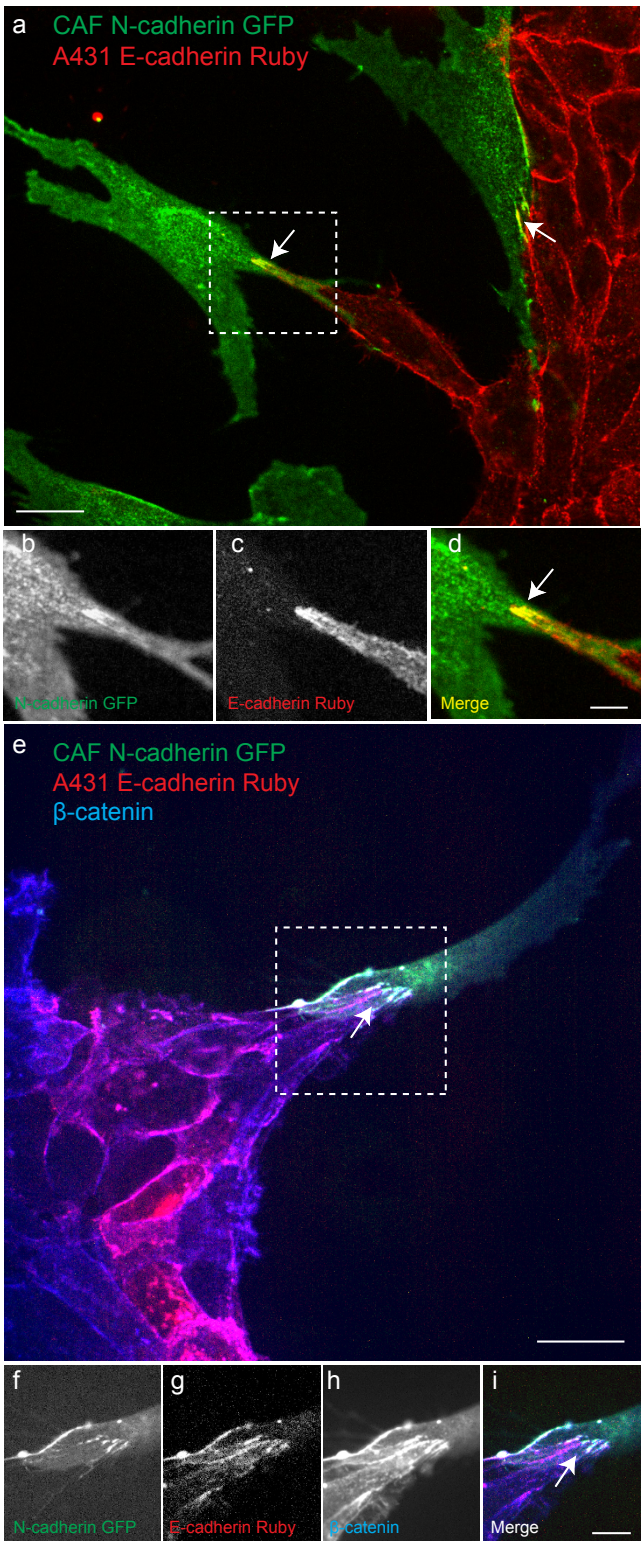

Supplementary Figure 3 Heterophilic E-cadherin/N-cadherin junctions between CAFs and A431 cells in the 2D spheroid assay. **(a)** Fluorescence images of a CAF expressing N-cadherin-GFP (green) contacting a spheroid of A431 cells expressing E-cadherin-Ruby (red) in the 2D spheroid assay on 6kPa gels. Scale bar, 20μm. White arrows show the presence of the E-cadherin/N-cadherin contact. **(b-d)** Magnified views of the region marked by a dashed box in **a**. Images representative of >4 samples. Scale bars, 5μm. **(e)** Fluorescence images of a CAF expressing N-cadherin-GFP (green) contacting a spheroid of A431 cells expressing E-cadherin-Ruby (red) in the 2D spheroid assay on 6kPa gels and stained for β-catenin (far-red). Scale bar, 20μm. White arrows point at the E-cadherin/N-cadherin contact. **(f-i)** Magnified views of the region marked by a dashed box in **e**. Images representative of >3 samples. Scale bars, 10μm.

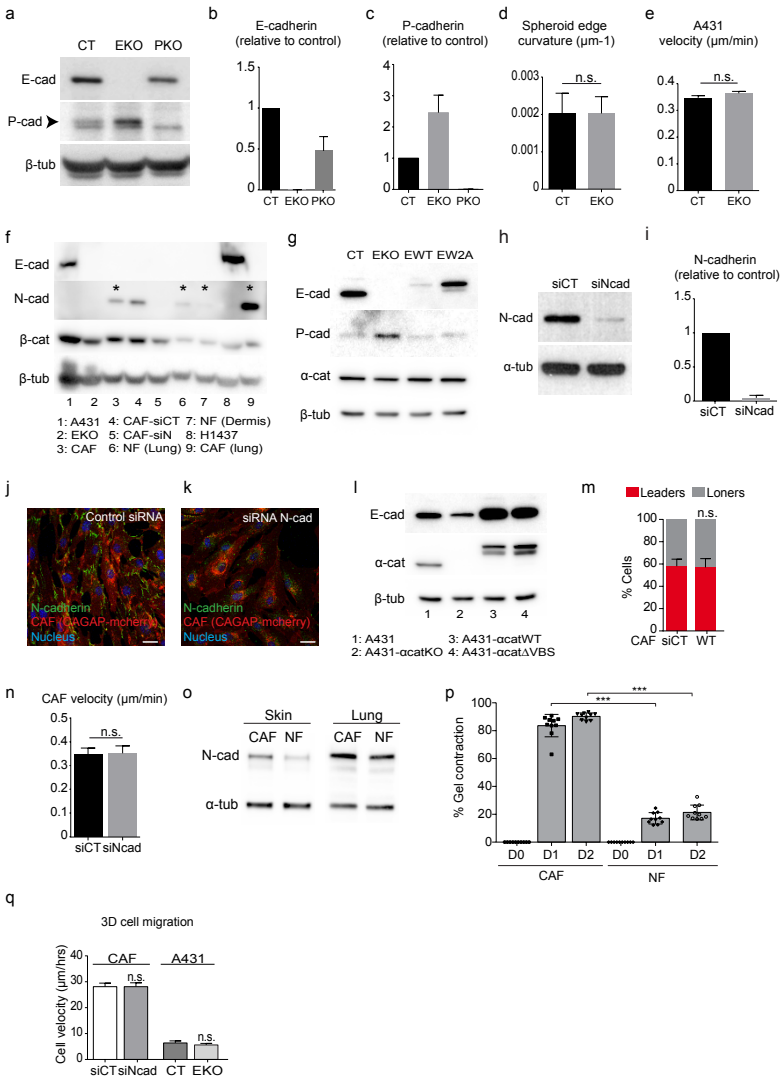

Supplementary Figure 4 Characterization of A431 cells types and CAFs. **(a)** Western blot of E-cadherin, P-cadherin and β-tubulin for A431 control cells (CT), A431-EcadKO cells (EKO), and A431-PcadKO cells (PKO). Image representative of 3 experiments. **(b,c)** Densitometric quantification of western blot bands relative to the loading (β-tubulin) of E-cadherin and P-Cadherin, respectively, for A431 control cells (CT), A431-EcadKO cells (EKO), and A431-PcadKO cells (PKO). The error bars represent mean +/- s.d. (n = 3 experiments). **(d,e)** Quantification of spheroid edge curvature and cancer cell velocity at the spheroid edge for control A431cells and A431-EcadKO cells in the absence of CAFs. No significant differences in cell velocity (P=0.993) and spheroid edge curvature (P=0.119) were observed between control cells and A431-EcadKO cells. For spheroid curvature, n=120 measurements from 3 independent experiments for A431 control cells, and n=265 measurements from 3 independent experiments for A431-EcadKO cells. For cell velocity, n=3 independent experiments (control, n=300 measurements; A431-EcadKO, n=400 measurements). The error bars represent s.e.m., n.s. indicates not significantly different, t-test. **(f)** Western blot of E-cadherin, N-cadherin, β-catenin and β-tubulin for A431 control cells (A431, column 1), A431-EcadKO (EKO, column 2), control vulval CAFs (CAF, column 3), vulval CAFs transfected with siRNA control (CAF-siCT, column 4), vulval CAF-siNcad (CAF-siN, column 5), normal lung fibroblasts (NF, column 6), normal dermal fibroblasts (NF, column 7), H1437 lung cancer cells (H1437, column 8), lung CAFs (CAF, column 9). Additional western blots are shown in figure **(o)** for the columns marked with asterisks. Image representative of 3 experiments. **(g)** Western blot of E-cadherin, P-cadherin, α-catenin and β-tubulin for A431 control cells (CT), A431-EcadKO cells (EKO), A431-EcadWT (rescue control) cells, and A431- EcadW2A cells. Image representative of 2 experiments. **(h)** Western blot of N-cadherin and α-tubulin for vulval CAFs-siCT and CAFs-siNcad. Image representative of 3 experiments. **(i)** Densitometric quantification of western blot bands relative to the loading (α-tubulin) of N-Cadherin for CAFs-siCT and CAFs-siNcad (n=3 experiments). The error bars represent s.d. **(j,k)** Representative fluorescence images of CAFs (CAGAP-mCherry) plated overnight on glass coverslips 3 days after siRNA transfection and fixed and stained for N-cadherin (green), and nucleus (blue). Image representative of 3 samples. Scale bars, 20 µm. **(l)** Western blot of E-cadherin, α-catenin and β-tubulin for A431 control cells (A431, column 1), A431-αcatKO (column 2), A431-αcatWT (rescue control, column 3), A431-αcatΔVBS (column 4). Image representative of 2 experiments. **(m)** Quantification of the fraction "leaders" or "loners" in vulval CAFs. No significant differences were found between CAFs-siCT and CAFs-WT. siCT, n=86 from 4 independent experiments; WT, n=57 from 3 independent experiments; n.s. indicates not significantly different (P=0.838), Mann-Whitney test. Error bars represent mean +/- s.e.m. **(n)** Quantification of velocity of isolated CAFs plated on fibronectin coated-6kPa gels transfected with siRNA Control (siCT, n=60) or si-Ncad (siNcad,n=63). Data were obtained from 3 independent experiments. n.s. indicates not significantly different (P=0.736), Mann-Whitney test. Error bars represent mean +/- s.e.m. **(o)** Western blot of N-cadherin (Ncad) and α-tubulin (α-tub) for CAFs and normal fibroblasts (NF) from skin and lung tissue. Image representative of 3 experiments. **(p)** Collagen gel contraction assay for vulval CAFs (CAF, n=10 measurements) and normal dermal fibroblasts (NF, n= 10 measurements). The percentage of gel contraction was measured immediately after gel polymerization (D0), 24 and 48 hours after gel polymerization, respectively (D1 and D2). Data were obtained from 3 independent experiments over at least 3 gels per condition per experiment. Error bars represent s.e.m., *** indicates P<0.0001, Mann-Whitney test. **(q)** Quantification of velocity in 3D ECM of isolated CAFs transfected with siRNA Control (siCT, n=158 cells) or si-N-cadherin (siNcad, n=143), P=0.788, and of isolated A431 control cells (CT, n=111) and A431-EcadKO cells (EKO, n=118), P=0.655. Data were obtained from 3 independent experiments. n.s. indicates not significantly different, Mann-Whitney test.

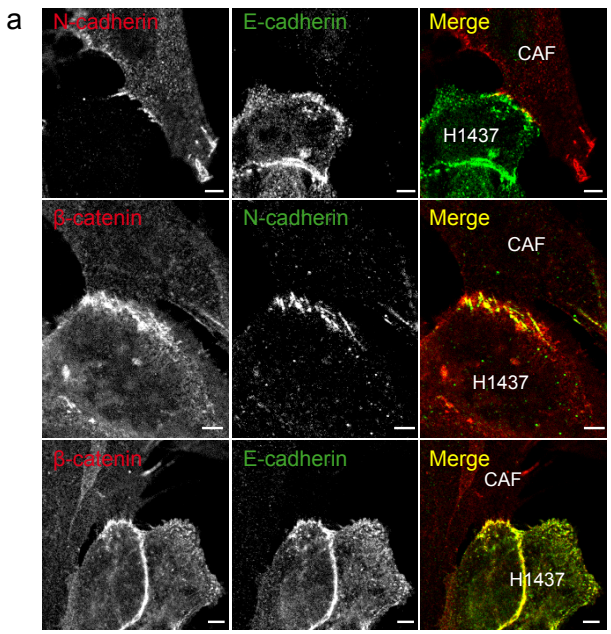

Supplementary Figure 5 The E-cadherin/N-cadherin junction is observed in vitro and in vivo **(a)** Co-culture of CAFs from one patient with lung adenocarcinoma and H1437 cells show E-cadherin/N-cadherin junctions. Image representative of 2 samples. Scale bars, 5μm.

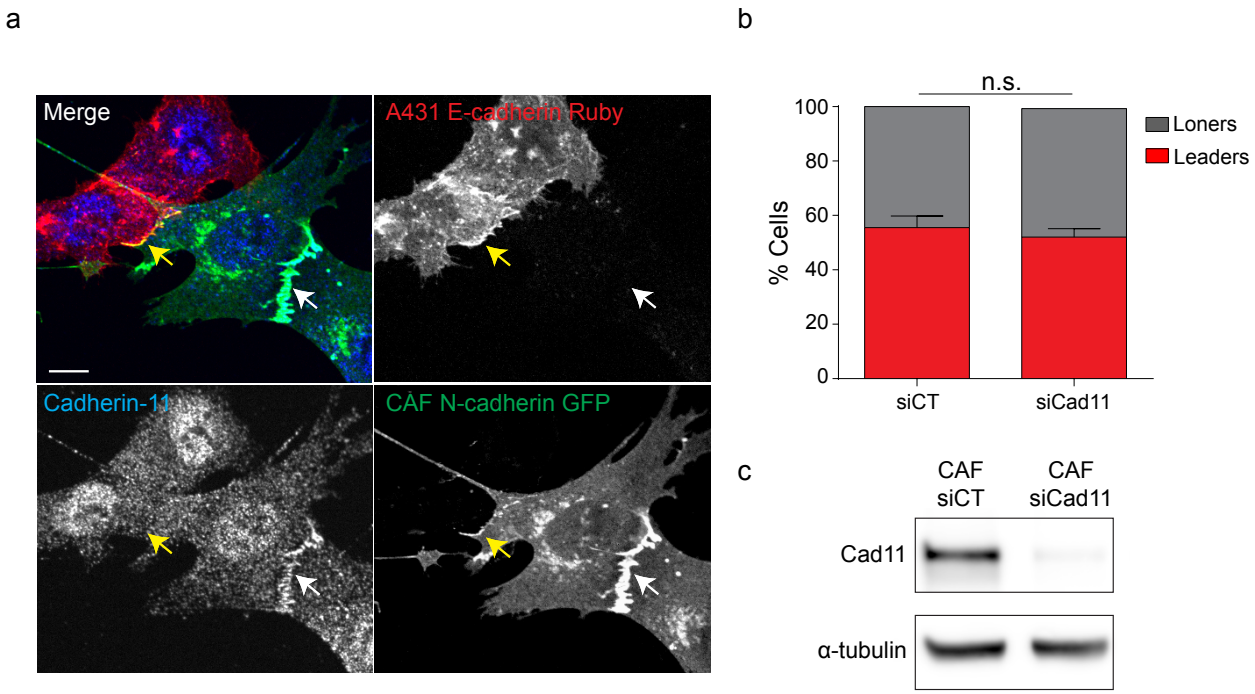

Supplementary Figure 6 Cadherin 11 is dispensable for CAF-led migration **(a)** Fluorescence images of vulval CAFs plated overnight on glass coverslips 3 days after siRNA transfection and fixed and stained for cadherin-11. Images representative of 2 experiments. Scale bar, 20 µm. **(b)** Quantification of the fraction of "leaders" or "loners" CAFs for CAFs transfected with siRNA-control (siCT) and CAF transfected with siRNA-cadherin11 (siCad11). No significant differences were found between the CAF-siCT and CAF-siCad11. siCT, n=147 CAFs, from 3 independent experiments; siCad11, n=201 CAFs, from 3 independent experiments. Error bars represent mean +/- s.e.m, n.s. indicates not significantly different, unpaired two-tailed t-test, P=0.584. **(c)** Western blot of cadherin-11 and α-tubulin for CAFs siCT and CAFs siCad11, Image representative of 3 experiments.

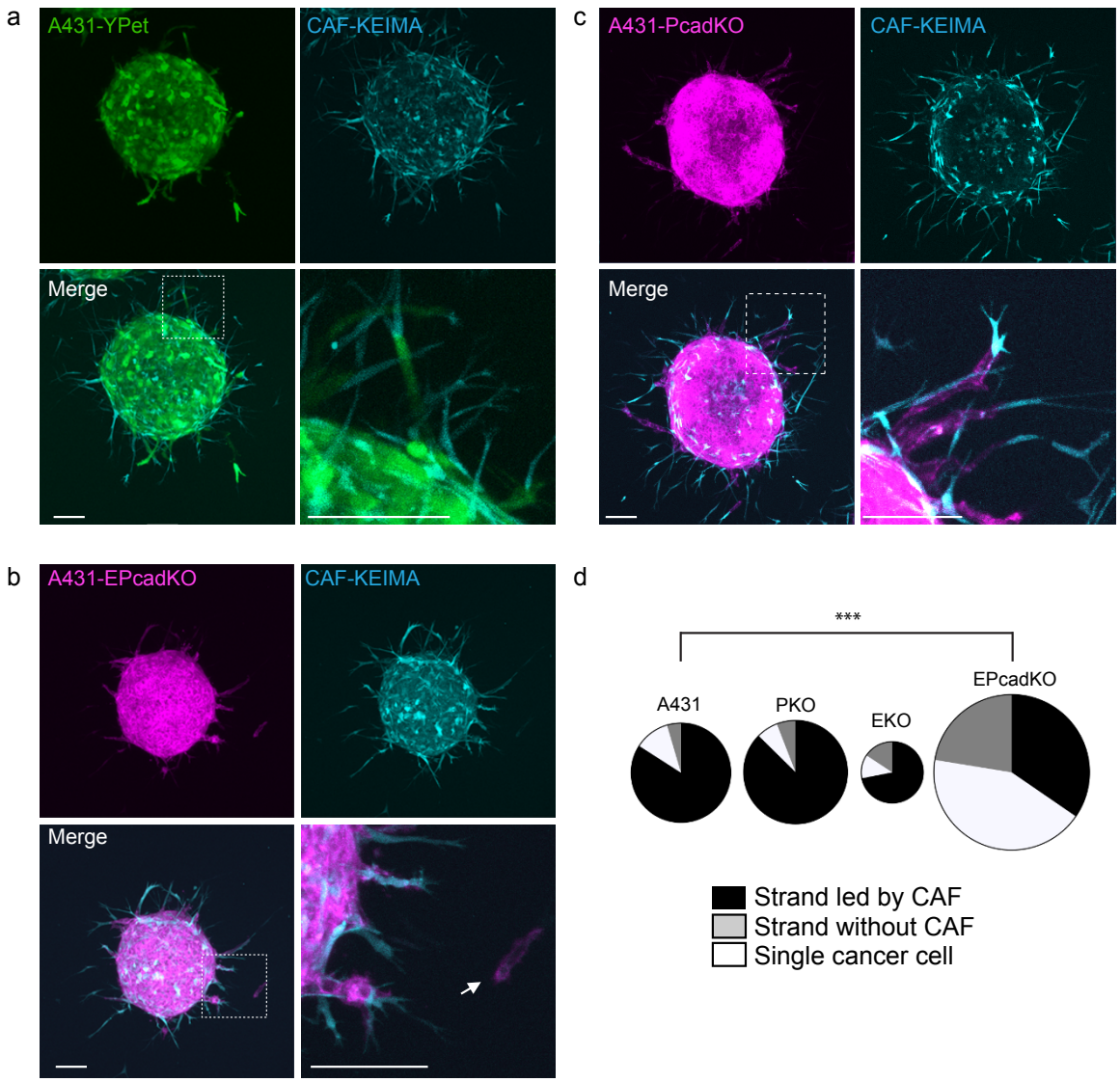

Supplementary Figure 7 The E/N-cadherin contact enables collective cancer cell invasion in 3D **(a,b)** Fluorescence images of spheroids containing different mixtures of CAFs and A431 cells after 60 hours of invasion in an organotypic ECM. **(a)** 1:1 mixture of A431-YPet (control) and control CAFs (KEIMA). **(b)** 1:1 mixture of A431-EPcadKO (mCherry) and control CAFs (KEIMA). **(c)** 1:1 mixture of A431-PcadKO (mCherry) and control CAFs (KEIMA). Images representative of >3 experiments. Scale bars, 100 µm. **(d)** Pie chart representation of the relative percentage of the 3 main modes of 3D invasion in our assays: strands led by CAFs (black), strands without CAFs (grey), and single cancer cells (white). The area of the circles is proportional to the total number of invasion events. A431, n=7, average number of total invasion events=6.29, A431 P-cadherin KO (PKO), n=18, average number of total invasion events=6.61, A431 E-cadherin KO, n=18, average number of total invasion events=1.78, A431 P-cadherin/E-cadherin double KO, n=8, average number of total invasion events=13.38. 3 independent experiments. Chi-squared test, *** indicates P<0.0001.

a

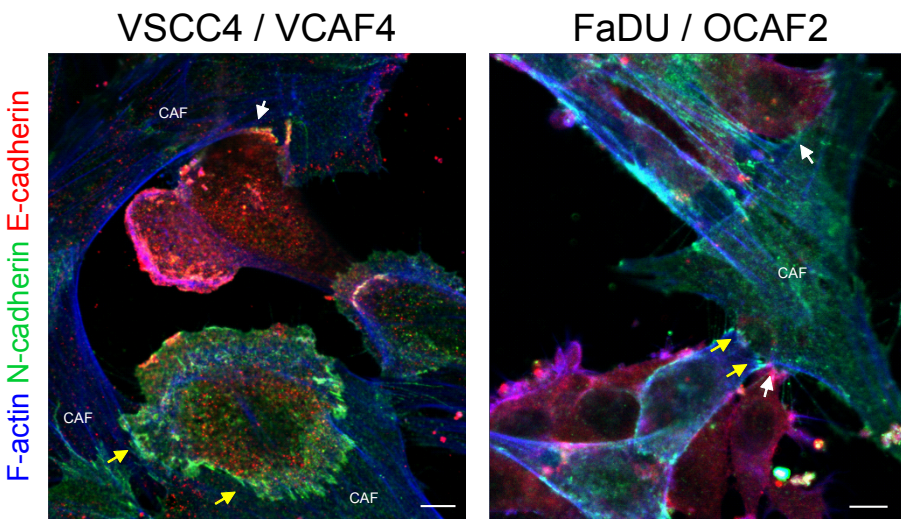

b

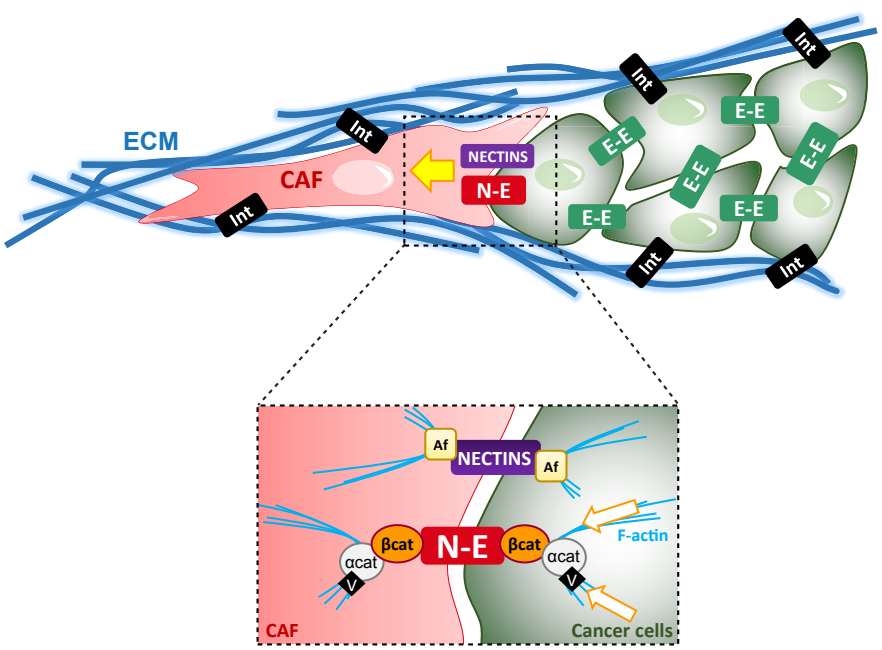

Supplementary Figure 8 coexistence of heterotypic and homotypic adhesion **(a)** Images show both homophilic N-cadherin junctions (yellow arrows) and heterophilic E-cadherin/N-cadherin junctions in co-cultures of cancer cells with variable endogenous N-cadherin levels. Left hand panel shows vulval SCC cells and CAFs isolated from the same patient and right hand panel shows FaDU SCC cells and oral SCC CAF (OCAF2). N-cadherin staining in green, E-cadherin in red, and F-actin in blue. Scale bar is 10μm. **(b)** Schematic representation of the role of cell-cell contacts in fibroblast-led cancer cell invasion. CAFs (elongated light red cells) engage extensively with the ECM and make heterophilic E-cadherin/N-cadherin junctions with cancer cells (light green cells). Heterophilic contacts and nectin/afadin complexes re-polarize CAFs to migrate away from the contact site (yellow arrows indicate directional cue). However, mechanical coupling via E-cadherin/N-cadherin and α-catenin/vinculin engagement leads to the dragging of cancer cells behind the CAF (white arrows with borders). This long-lived contact continually promotes CAF migration. Af, afadin; v, vinculin; αcat, α-catenin; βcat, β-catenin; N-E, N-cadherin/E-cadherin junction; E-E, E-cadherin/E-cadherin junction; Int, integrin.

Blots from Sup.Figure4a

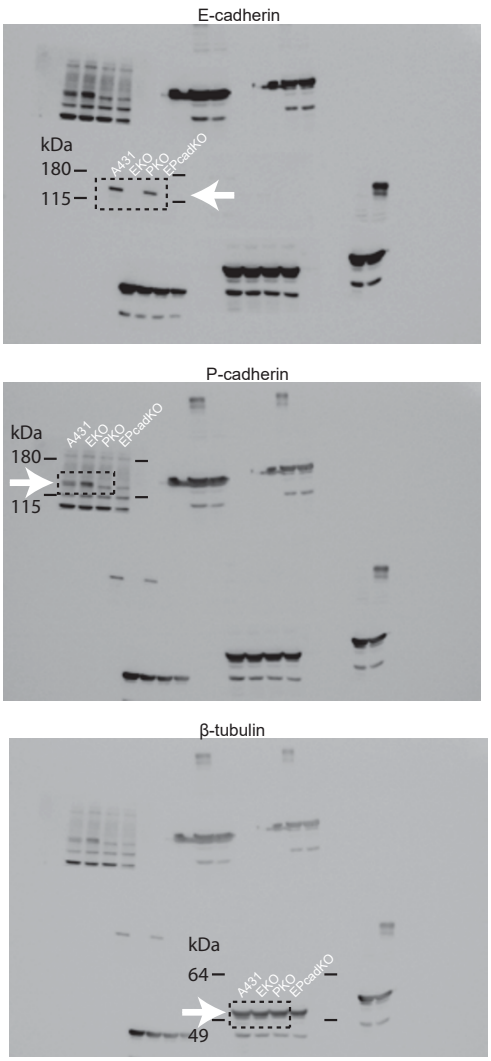

Blots from Sup.Figure4f

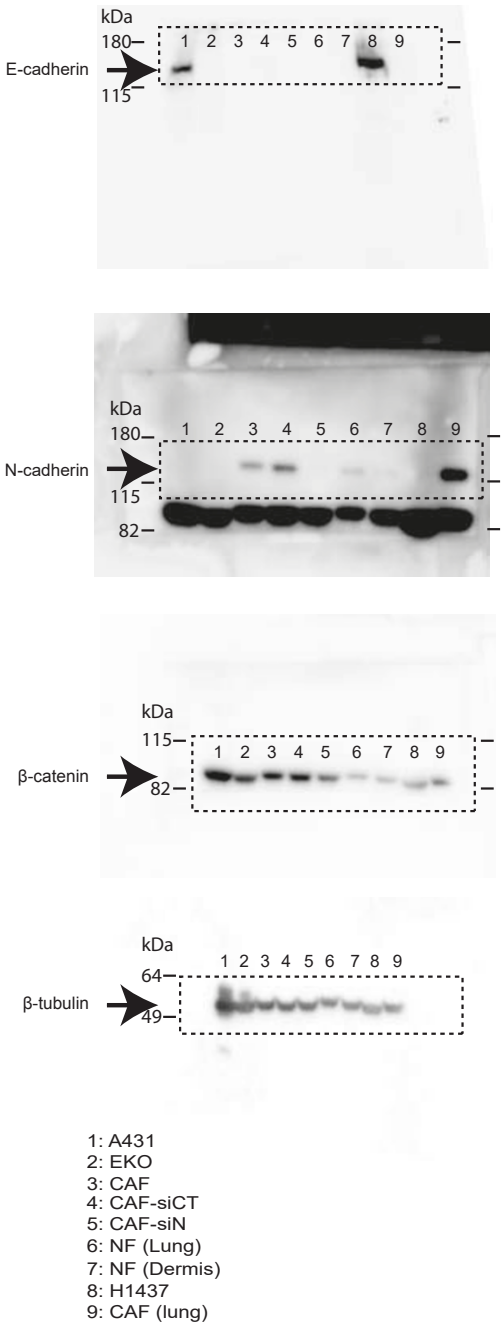

1: A431
2: EKO
3: CAF
4: CAF-siCT
5: CAF-siN
6: NF (Lung)
7: NF (Dermis)
8: H1437
9: CAF (lung)

Supplementary Figure 9 Unprocessed Western blot scans.

Blots from Sup. Figure 4g and l

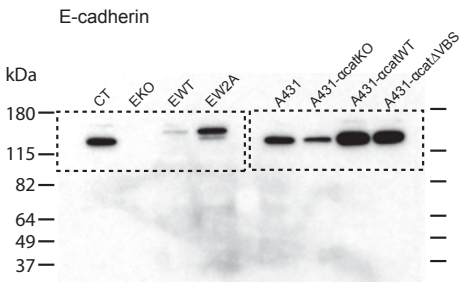

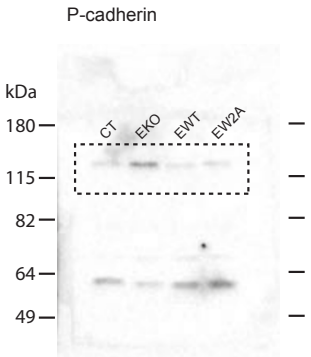

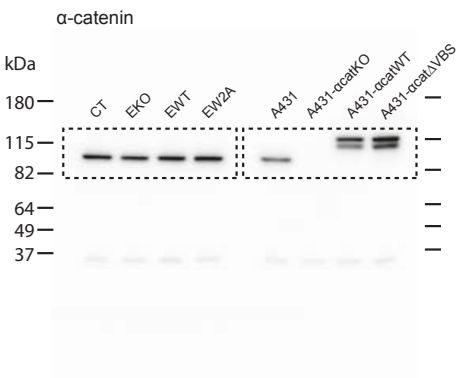

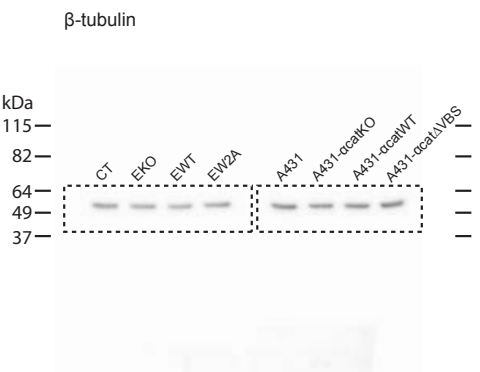

Blots from Sup. Figure 4h

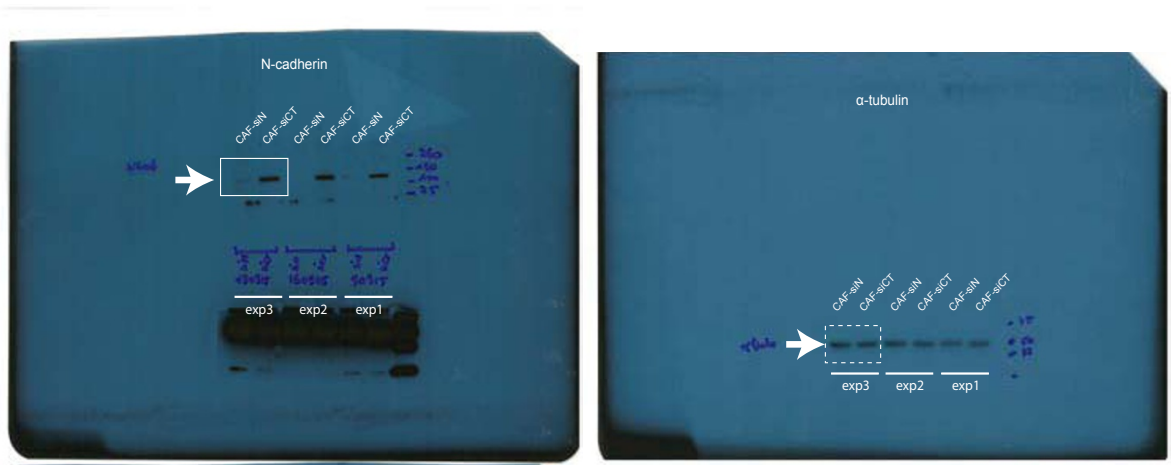

Supplementary Figure 9 Continued

Blots from Sup. Figure 4o

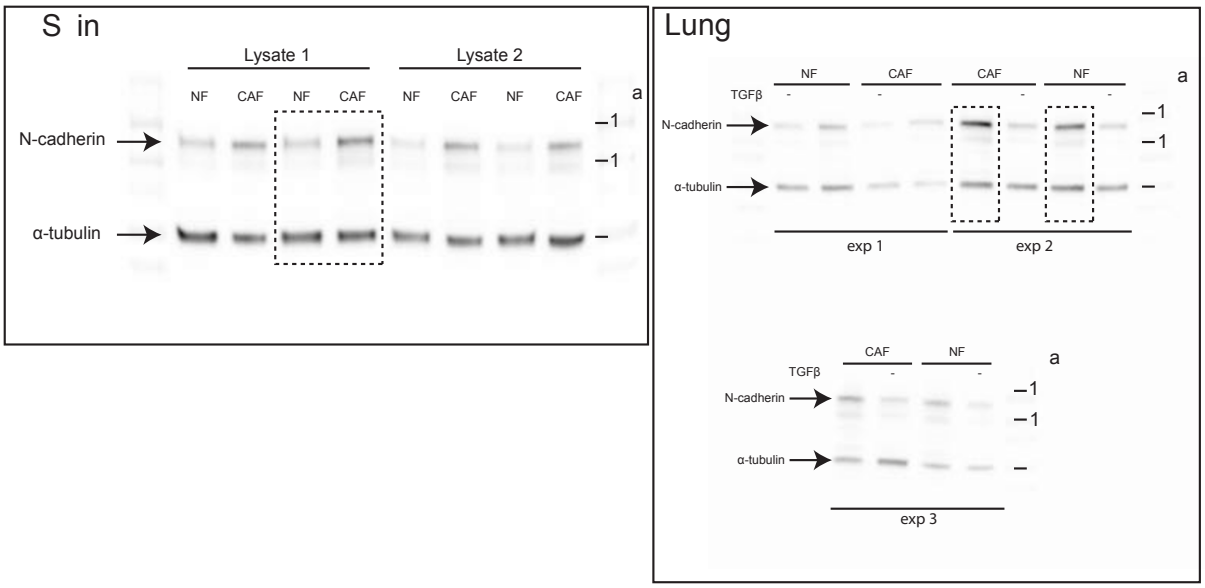

Blots from Sup. Figure c

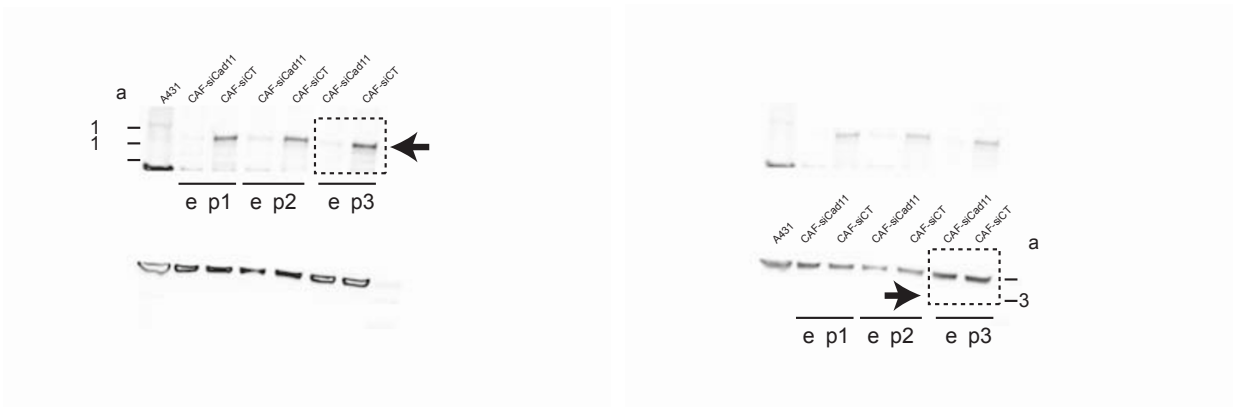

Blots from Sup. Figure f

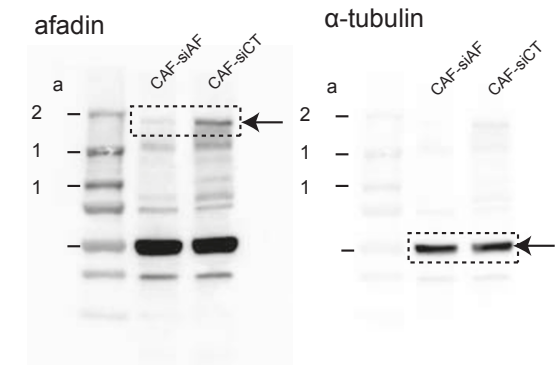

Supplementary Figure 9 Continued

Supplementary Tables Legends

Supplementary Table 1 Statistical details of Fig. 4 panels.

Supplementary Videos Legends

Supplementary Video 1 CAFs lead cancer cell strands in 3D invasion assays. Representative 3D rendering of a fixed spheroid containing vulval CAFs (VCAF, CAGAP-cherry) and A431 cells (green) (ratio 1:1) after 24 hours embedded in an organotypic ECM. z-step, 0.25µm.

Supplementary Video 2 CAFs favor expansion of cancer cell spheroids in 2D. Representative time-lapse of a 2D migration assay on a soft polyacrylamide substrate (Young's modulus E=6kPa). White rectangles highlight three CAFs (CAGAP-mcherry) leading the expansion of the A431 spheroid (unlabeled). Images were acquired every 5 min. Scale bar, 100µm.

Supplementary Video 3 CAFs lead collective migration of cancer cells in 2D. Representative time-lapse of one CAF (CAGAP-mcherry) leading the 2D migration of A431 cells (unlabeled) away from the spheroid edge. Cells are adhered on an elastic substrate (Young's modulus E=6kPa). Images were acquired every 5 min. Scale bar, 2µm.

Supplementary Video 4 FIB-SEM reveals multiple contact points at the CAF-A431 interface. Representative FIB-SEM z-stack sequence of areas of contact between CAFs (VCAF) and A431 cells. White arrows show the location of contact between CAF and cancer cells. Image dimensions, 10×12 µmm, z-stack steps 50nm.

Supplementary Video 5 W2A mutation in the extracellular domain of E-cadherin drastically diminishes co-localization with N-cadherin. Representative confocal time-lapse movie of A431-EcadWT-Ruby or A431-EcadW2A-Ruby cells co-cultured with CAFs expressing N-cadherin-GFP. Dynamics of the co-culture was recorded at 5 min intervals. Scale Bar, 20 µm.

Supplementary Video 6 Calcium chelation abrogates reversibly E-cadherin/N-cadherin co-localization. Representative confocal time-lapse movie of A431-E-cadherin-Ruby mixed with CAF-N-cadherin-GFP showing dynamics of the E-cadherin/N-cadherin contact during a calcium chelation assay. After 10 minutes of acquisition, the EGTA solution was added to the medium (final concentration, 4mM). After 4 min incubation, the medium containing EGTA was washed three times with normal medium. Arrows show the formation of the E-cadherin/N-cadherin contact after washout of EGTA. Images were acquired every 2 min. Scale Bar, 20µm.

Supplementary Video 7 Dynamics of the E-cadherin/N-cadherin adhesion during CAF-led cancer cell migration. Representative confocal time-lapse movie of A431-E-cadherin-Ruby spheroid seeded on glass and surrounded by CAF-N-cadherin-GFP. The magnified panel represents the area of contact between the leading CAF and A431 cells. White arrow shows the location of the E-cadherin/N-cadherin contact. Images were acquired every 5 min. Scale Bars, 20µm (right panel), 10µm (left panel).

Supplementary Video 8 E-cadherin and β-catenin colocalize at heterotypic contacts. Representative confocal time-lapse movie of A431-E-cadherin-Ruby expressing β-catenin-GFP mixed with unlabeled CAFs. The magnified panel represents the area of contact between the leading CAF and the A431 cells. The white arrow shows the localization of the contact between the A431 cells and the CAF (white asterisk). Images were acquired every 2 min. Scale Bar, 10µm.

Supplementary Video 9 E-cadherin and vinculin colocalize at heterotypic contacts. Representative confocal time-lapse movie of A431-E-cadherin-Ruby expressing vinculin-GFP mixed with unlabeled CAFs. The white arrow shows the localization of the contact between the A431 cells and the CAF (white asterisk). Note an enrichment of E-cadherin (red) and vinculin (green) at the contact. Images were acquired every 2 min. Scale Bar,10µm.

Supplementary Video 10 CAFs exert pulling forces on cancer cells. Representative time-lapse of a CAF (CAGAP-mcherry) dragging A431 cells. The magnitude and direction of the force exerted by the CAF on the cancer cell is represented by the green vector. For clarity, the force vector is represented at the geometric center of the CAF. See Figure 5 for a quantification of the force throughout the time-lapse. Scale bar, 50 µm.

Supplementary Video 11 E-cadherin is required for force transmission between CAFs and A431 cells. Representative time-lapse of a CAF contacting the edge of A431-EcadKO cells. The magnitude and direction of the force exerted by the CAF on the cancer cell is represented by the green vector. For clarity, the force vector is represented at the geometric center of the CAF. See Figure 5 for a quantification of the force throughout the time-lapse. Scale bar, 50 µm.

Supplementary Video 12 "Leader" vs "loner" CAF phenotypes.
Representative time-lapse of a "leader" CAF (left) and a "loner" CAF (right) (CAGAP-mcherry, white arrow). Images were acquired every 5 min. Scale bars, 20µm.

Supplementary Video 13 The heterotypic contact regulates CAF repolarization. Representative time-lapse of a control CAF (left panel) or N-cadherin depleted CAF (CAF-siNcad, right panel) contacting the edge of a spheroid of A431 control cells (left and right panel) or A431-EcadKO cells (middle panel). Colored spots show the location of the CAFs. Images were acquired every 10 min. Scale bar, 50 µm.